Biogeosciences, 17, 5513–5537, 2020
https://doi.org/10.5194/bg-17-5513-2020

Biogeosciences
Open Access
EGU

N_2O isotope approaches for source partitioning of N_2O production and estimation of N_2O reduction – validation with the ^{15}N gas-flux method in laboratory and field studies

Dominika Lewicka-Szczebak[1,2], Maciej Piotr Lewicki[3], and Reinhard Well[4]

[1]Centre for Stable Isotope Research and Analysis, University of Göttingen, Büsgenweg 2, 37077 Göttingen, Germany
[2]Institute of Geological Sciences, University of Wrocław, pl. M. Borna 9, 50-204 Wrocław, Poland
[3]Institute of Theoretical Physics, University of Wrocław, pl. M. Borna 9, 50-204 Wrocław, Poland
[4]Climate-Smart Agriculture, Thünen-Institut, Bundesallee 65, 38116 Braunschweig, Germany

Correspondence: Dominika Lewicka-Szczebak (dominika.lewicka-szczebak@uwr.edu.pl)

Received: 4 June 2020 – Discussion started: 11 June 2020
Revised: 23 September 2020 – Accepted: 5 October 2020 – Published: 14 November 2020

Abstract. The approaches based on natural abundance N_2O stable isotopes are often applied for the estimation of mixing proportions between various N_2O-producing pathways as well as for estimation of the extent of N_2O reduction to N_2. But such applications are associated with numerous uncertainties; hence, their limited accuracy needs to be considered. Here we present the first systematic validation of these methods for laboratory and field studies by applying the ^{15}N gas-flux method as the reference approach.

Besides applying dual-isotope plots for interpretation of N_2O isotopic data, for the first time we propose a three dimensional N_2O isotopocule model based on Bayesian statistics to estimate the N_2O mixing proportions and reduction extent based simultaneously on three N_2O isotopic signatures ($\delta^{15}N$, $\delta^{15}N^{SP}$, and $\delta^{18}O$). Determination of the mixing proportions of individual pathways with N_2O isotopic approaches often appears imprecise, mainly due to imperfect isotopic separation of the particular pathways. Nevertheless, the estimation of N_2O reduction is much more robust, when applying an optimal calculation strategy, typically reaching an accuracy of N_2O residual fraction determination of about 0.15.

1 Introduction

Nitrous oxide (N_2O) emission from soils and waters may result from numerous nitrogen transformation processes, mainly heterotrophic bacterial denitrification (bD), autotrophic nitrification (Ni), nitrifier denitrification (nD), and fungal denitrification (fD), but also heterotrophic nitrification, chemodenitrification, or co-denitrification (Butterbach-Bahl et al., 2013; Firestone and Davidson, 1989; Müller et al., 2014). The ability to distinguish the proportional contributions of these various N_2O origins (f_{bD}, f_{Ni}, f_{nD}, f_{fD}) is important for constraining the N budget and for developing and assessing the performance of mitigation strategies for N_2O emission, which significantly contributes to global warming and stratospheric ozone depletion (IPCC, 2007; Ravishankara et al., 2009). Determination of the mixing proportions f_{bD}, f_{Ni}, and f_{nD} is only partially possible by combination of numerous experimental techniques, including sophisticated ^{15}N and ^{18}O isotope labeling techniques (Müller et al., 2014; Wrage-Mönnig et al., 2018). However, also natural abundance N_2O isotopic analyses have been often applied to estimate the possible proportional contribution of particular pathways (Toyoda et al., 2017; Yu et al., 2020) and are currently the only isotopic approach to identify f_{fD} (Rohe et al., 2017; Wrage-Mönnig et al., 2018).

The determination of mixing proportions based on natural abundance N_2O isotopes is theoretically possible thanks to characteristic isotopic fractionation for each pathway, determined in numerous laboratory pure culture experiments

(Toyoda et al., 2017), but is practically very complex, mainly due to changes in N_2O isotopic signature during its partial reduction to N_2 and due to overlapping isotopic endmember values of individual pathways. N_2O isotopic analyses comprise the isotopic determination of oxygen ($\delta^{18}O$), bulk nitrogen ($\delta^{15}N$), and nitrogen site preference ($\delta^{15}N^{SP}$), i.e., the difference in $\delta^{15}N$ between the central and the peripheral N atom of the linear N_2O molecules (Brenninkmeijer and Röckmann, 1999; Toyoda and Yoshida, 1999). These three isotopic signatures ($\delta^{18}O$, $\delta^{15}N$, and $\delta^{15}N^{SP}$) show characteristic ranges of isotopic signatures for particular N_2O production pathways but are also altered during the N_2O reduction process.

N_2O reduction to N_2 occurs during the last step of microbial denitrification, i.e., anoxic reduction of nitrate (NO_3^-) to N_2 through the following intermediates: $NO_3^- \rightarrow NO_2^- \rightarrow NO \rightarrow N_2O \rightarrow N_2$ (Firestone and Davidson, 1989; Knowles, 1982). Commonly applied experimental techniques enable us to quantitatively analyze only the intermediate product of this process, N_2O, but not the final product, N_2 (Groffman, 2012; Groffman et al., 2006). This is due to the high atmospheric N_2 background precluding direct measurements of N_2 emissions in the presence of the natural atmosphere (Bouwman et al., 2013; Saggar et al., 2013). Estimation of N_2 flux is possible with sophisticated laboratory experiments applying a N_2-free helium atmosphere (Scholefield et al., 1997) or the ^{15}N gas-flux method, i.e., ^{15}N analyses of gas fluxes after addition of a ^{15}N-labeled substrate (Bergsma et al., 2001; Schmidt et al., 1998). Previous studies documented large possible variations in N_2 flux and consequently also in the residual unreduced N_2O fraction: $r_{N_2O} = y_{N_2O}/(y_{N_2} + y_{N_2O})$ (y: mole fraction). In laboratory studies, the whole scale of possible r_{N_2O} variations, ranging from 0 to 1, has been found (Lewicka-Szczebak et al., 2017; Lewicka-Szczebak et al., 2015; Mathieu et al., 2006; Morse and Bernhardt, 2013; Senbayram et al., 2012). Due to technical limitations, so far only the ^{15}N gas-flux method had been applied in field conditions to determine r_{N_2O} (Aulakh et al., 1991; Baily et al., 2012; Bergsma et al., 2001; Buchen et al., 2016; Decock and Six, 2013; Kulkarni et al., 2013; Mosier et al., 1986). Moreover, the first attempt to apply the ^{15}N gas-flux method under N_2-reduced atmosphere in the field has been presented recently (Well et al., 2019a). This new approach increases the sensitivity of the ^{15}N gas-flux method (80-fold better sensitivity for $N_2 + N_2O$ flux measurements; Well et al., 2019a), which was so far very limiting for successful application in field studies (Buchen et al., 2016). But still, application of this approach is technically very demanding and applicable only with a low temporal and spatial resolution. Hence, no comprehensive datasets from field-based measurements of soil N_2 emissions are available, and this important component in the soil nitrogen budget is still missing. This constitutes a serious shortcoming in understanding and mitigating the microbial consumption of nitrogen fertilizers (Bouwman et al., 2013; Seitzinger, 2008) and the N_2O budget.

An alternative approach for assessing N_2 fluxes is the use of N_2O isotopes, which allows researchers to indirectly determine r_{N_2O} from the isotopic signature of the residual N_2O (Ostrom et al., 2007; Well and Flessa, 2009), since the increase in $\delta^{18}O$, $\delta^{15}N$, and $\delta^{15}N^{SP}$ of the residual N_2O due to N_2O reduction is related to r_{N_2O} (Jinuntuya-Nortman et al., 2008; Menyailo and Hungate, 2006; Ostrom et al., 2007; Well and Flessa, 2009). This approach is also potentially applicable for quantification of r_{N_2O} in field conditions (Buchen et al., 2018; Park et al., 2011; Toyoda et al., 2011; Verhoeven et al., 2019; Zou et al., 2014). Its advantage over the ^{15}N gas-flux method lies in its easier and noninvasive application, no need of additional fertilization, and much lower costs. But, on the other hand, complexity of the N_2O production pathways with co-occurring N_2O reduction, variability of isotope effects, and isotope fractionation associated with diffusion processes can make this estimation imprecise (Lewicka-Szczebak et al., 2015; Lewicka-Szczebak et al., 2014; Yu et al., 2020). Since mostly two processes, mixing and reduction, determine the final N_2O isotopic signature, we need at least two isotopic values to be able to assess both N_2O mixing proportions of two N_2O production pathways and r_{N_2O}. Therefore, the dual-isotope plots are often applied, which is also called the isotope mapping approach (MAP), i.e., isotopic relations in the space $\delta^{15}N^{SP}/\delta^{15}N$ (SP/N MAP) and $\delta^{15}N^{SP}/\delta^{18}O$ (SP/O MAP). The SP/N MAP was first applied for agricultural soils by Toyoda et al. (2011). Afterwards many studies utilized this relationship to determine N_2O mixing proportions and N_2O reduction (Kato et al., 2013; Wolf et al., 2015; Zou et al., 2014). Later, it was shown that $\delta^{18}O$ can be also used as a good tracer for N_2O production processes, thanks to high O exchange during bD, resulting in quite stable $\delta^{18}O$ values for this pathway (Lewicka-Szczebak et al., 2016). Based on this finding, the SP/O MAP for N_2O interpretation was proposed (Lewicka-Szczebak et al., 2017) and applied in recent studies (Buchen et al., 2018; Ibraim et al., 2019; Verhoeven et al., 2019; Wu et al., 2019). Both SP/N MAP and SP/O MAP have been applied jointly for field studies (Ibraim et al., 2019) and showed quite a good agreement between the calculated r_{N_2O} and f_{bD} values. However, so far these two approaches were not combined together into a complex three-dimensional model allowing the calculation of pathway mixing proportions and r_{N_2O} based on three isotopic signatures ($\delta^{15}N$, $\delta^{18}O$, $\delta^{15}N^{SP}$) simultaneously. Development of such a model is a clear current need.

Precise quantification of both the production pathway proportions and the extent of N_2O reduction with isotope MAPs is limited by wide ranges of isotopic signatures reported for individual pathways, the overlapping of these isotopic signatures ranges, variations in substrate isotopic compositions, and variability of fractionation factors associated with N_2O reduction (Toyoda et al., 2017; Yu et al., 2020). Hence, it can be questioned how far we can trust the quantitative results provided by calculations based on isotope MAPs. To answer

this question, comparisons with estimates based on independent methods are needed. The first attempt at comparing r_{N_2O} obtained with SP/O MAP and the ^{15}N gas-flux method in a field case study was performed by Buchen et al. (2018). Due to nonidentical treatment (different fertilizer application procedures: needle injection of fertilizer solution for ^{15}N treatments and surface distribution of fertilizer in natural abundance (NA) treatments; different sizes of ^{15}N and NA microplots and chambers) and the consequent differences in soil moisture and mineral N, the results of both treatments were difficult to compare; however, the r_{N_2O} values obtained clearly indicated the dominance of N_2 flux over N_2O flux by both methods. That study also presented analysis of various calculation scenarios applying upper and lower limits for mixing isotopic endmember values and reduction fractionation factors, which revealed pronounced uncertainty in this calculation approach (Buchen et al., 2018). It was suggested that a further study on validation and uncertainty analysis of the SP/O MAP is required with particular attention to identical treatment for both approaches under comparison. Another comparison was performed with archival datasets applying helium incubations as a reference method and indicated large uncertainties in the calculations based on the SP/O MAP (Wu et al., 2019). The huge uncertainties determined in these studies resulted from the fact that the full range of endmember values and fractionation factors reported in the literature was taken into account. But for particular soils and experimental conditions these ranges might be smaller and uncertainties thus lower. Hence, it is still unsure to which extent the ranges of isotopic fractionation factors determined in laboratory conditions and for pure culture studies are valid for particular experiments. It is not feasible to validate each isotope characteristic separately in field studies, since the pathways are not easily separable, and this can be only achieved in controlled laboratory conditions.

While these recent studies indicated low precision associated with the r_{N_2O} estimations based on N_2O isotopocule approaches (Buchen et al., 2018; Wu et al., 2019), the suitability of this approach in estimating r_{N_2O} and mixing proportions has never been validated in a systematic study with a reference method. Hence, the idea of this study is to validate the methods based on N_2O isotope MAPs and determine their attainable precision by parallel application with the reference method – the ^{15}N gas-flux method. We compare the calculated N_2 flux based on the ^{15}N gas-flux method (^{15}N treatment) and N_2O isotope MAPs (natural abundance (NA) treatment) in laboratory and field experiments by applying an identical treatment strategy (meaning identical fertilizer application procedure: fertilizer solution applied with needle injection technique, identical water and fertilizer addition, and identical plots and chamber sizes). Moreover, we present a new three-dimensional isotopocule model (3DIM) based on 3D isotopocule space and provide a validation of its outputs. This is the first attempt to systematically validate the results from N_2O natural abundance isotopic studies (N_2O isotopocule approaches) in laboratory and field conditions.

Our aim is to (1) validate applicability of N_2O isotopocule approaches for N_2 flux determination, (2) validate the applicability of N_2O isotopocule approaches to partition N_2O production pathways, and (3) to develop the best evaluation strategy for interpretation of N_2O isotopic data.

2 Methods

2.1 Field study

Silt loam soil *Albic Luvisol* from arable cropland of Merklingsen experimental station located near Soest (North Rhine-Westphalia, Germany; 51°34′15.5″ N, 8°00′06.8″ E) was used (87 % silt, 11 % clay, 2 % sand). The soil density of intact cores was 1.3 g mL^{-1}, pH value was 6.8, total C content was 1.30 %, total N content was 0.16 %, and organic matter content was 2.14 %. The field was sown with winter rye in September 2015 and mineral underfoot fertilization was applied. Our experiments were conducted on experimental plots of a field study on management effects on greenhouse gas fluxes. We selected the "climate-optimized farm" treatment where a complex cropping rotation of silage maize, winter wheat, faba bean, winter barley, and perennial rye had been established since 2010 (Kramps-Alpmann et al., 2017). This treatment was managed by zero tillage with direct seeding, and fertilization was a combination of organic (biogas digestate) and mineral fertilizer where doses were set according to official fertilizer recommendations (Baumgärtel and Benke, 2009). On 13 October in each of the four replicate plots (6 m × 12 m), we established microplots consisting of aluminum cylinders (length 35 cm, diameter 15 cm) inserted to 30 cm depth into the soil so that 5 cm extended above the ground for installation of the flux chamber. Three field campaigns were carried out in November 2015 (F1), March 2016 (F2), and May/June 2016 (F3). After each field campaign the cylinders were removed, cleaned, and later reinstalled at new locations (on 27 November 2015 for F2 sampling and on 28 April 2016 for F3 sampling) for the next field campaign.

On each replicate plot, cylinders were installed pairwise – one for gas-flux measurements and one for mineral nitrogen sampling – for three treatments – natural abundance (NA), traced nitrate ($^{15}NO_3^-$), and traced ammonium ($^{15}NH_4^+$) – which is in total six cylinders per replicate plot. The distance between each treatment cylinder was at least 2 m; the pair of cylinders for one treatment were separated by 0.5 m distance.

At the beginning of the experiment, a fertilizer solution with 240 mg N L^{-1} as $NaNO_3$ and 240 mg N L^{-1} as NH_4Cl was added to the experimental microplots with the needle injection technique. Three milliliters of the fertilizer solution was injected into 72 points using 12 needles inserted subsequently into six depths (2.5, 7.5, 12.5, 17.5,

22.5, and 27.5 cm) from the top to the bottom using peristaltic pump. This strategy was based on previous studies (Buchen et al., 2016; Wu et al., 2011) and was enhanced by pre-experimental tests to obtain the most homogeneous tracer distribution (Lewicka-Szczebak and Well, 2020). Total fertilization was 20 mg N per kg soil (added as $NaNO_3$ (10 mg N) and NH_4Cl (10 mg N)), which was equivalent to about 80 kg N ha^{-1}.

In total, 216 mL of fertilizing solution was inserted into each microplot, which resulted in a 3 % increase in water content. For ^{15}N-labeled treatments, the ^{15}N content in fertilizing solution was calculated to achieve about 60 at. % (atomic percent) ^{15}N in the ^{15}N-labeled N pool. The $^{15}NO_3^-$ treatment received tracer solution containing 68 at. % ^{15}N, and the $^{15}NH_4^+$ treatment received 64 at. % ^{15}N.

Immediately after fertilizing solution addition, the flux chamber microplots were closed for gas accumulation. Opaque PVC chambers of an area of 1.767 dm^2 and a volume of 2.65 dm^3 were applied with installed valves for sample collection and a fan for gas mixing. The closed chamber method (Hutchinson and Mosier, 1981) was used for N_2O flux measurement. Chambers were closed and sealed with airtight rubber bands for 120 min, and headspace sampling was performed after 40, 80 and 120 min into evacuated crimped 20 mL vials with a 30 mL syringe for gas-flux measurements. Additionally, after 120 min, samples for isotope analysis were collected. For ^{15}N treatments, two identical replicates were taken into 12 mL evacuated screw-cap Exetainers® (Labco Limited, Ceredigion, UK) with two combined 15 mL syringes. For the NA treatment, one gas sample was transferred into an evacuated 115 mL crimp-cap vial with a 150 mL syringe.

Each field campaign lasted 5 d. Gas samples were collected once on the first day after fertilization, afterwards twice a day – in the morning and in the evening, and once on the last 5th day in the morning.

The soil sampling microplots were treated identically and used for mineral nitrogen sampling. The soil samples were collected with a Goettinger boring rod with 18 mm outer diameter and 14 mm slots (Nietfeld GmbH, Quakenbrück, Germany). Boreholes were sealed by inserting a closed sand-filled PVC pipe with the same diameter as the bore. For each sampling, three cores were collected and homogenized to one mixed sample each day; hence, we performed five soil samplings during each campaign. The samples were immediately transported to the laboratory at 6 °C, and mineral nitrogen extractions were performed on the same day.

2.2 Laboratory incubation

The soil from the experimental field site was used to prepare incubation columns for laboratory incubation. The soil, upper 30 cm layer, was collected on the 18 January 2018 from the experimental plot used previously for field campaigns, and the incubation was conducted from 19 February 2018 to 5 March 2018. The soil was air-dried and sieved at 4 mm mesh size. Afterwards, the soil was rewetted to achieve a water content equivalent to 60 % water-filled pore space (WFPS) and fertilized with 20 mg N per kg soil, added as $NaNO_3$ (10 mg N) and NH_4Cl (10 mg N). Analogically as in the field study, three treatments were prepared: natural abundance (NA), labeled with ^{15}N nitrate ($^{15}NO_3$), and labeled with ^{15}N ammonium ($^{15}NH_4$). For the $^{15}NO_3$ treatment, $NaNO_3$ solution with 72 at. % ^{15}N was added, and for the $^{15}NH_4$ treatment, NH_4Cl solution with 63 at. % ^{15}N was added. Then soils were thoroughly mixed to obtain a homogenous distribution of water and fertilizer and an equivalent of 1.69 kg dry soil was repacked into each incubation column with a bulk density of 1.3 g cm^{-3}.

For each treatment, 14 columns were prepared, and half of them received additional water injected into the top of the column (100 mL water added) to prepare two moisture treatments: dry (61 % WFPS) and wet (72 % WFPS). The incubation lasted 12 d. In the meantime, on the 6th day of incubation, water addition on the top of each column was repeated (80 mL water added) to increase the soil moisture in both treatments to ca. 68 % WFPS in the dry treatment and ca. 81 % WFPS in the wet treatment. The WFPS values were controlled during the experiment (Fig. S1 in the Supplement). The strategy of adding water on the top of the column to achieve target water content was necessary to allow for mixing and compaction at a suitable (low) water content of the soil and thus to optimize homogeneity of water and fertilizer distribution (Lewicka-Szczebak and Well, 2020). The incubation temperature was 20 °C. The columns were continuously flushed with a gas mixture with reduced N_2 content to increase the measurement sensitivity (2 % N_2 and 21 % O_2 in He; Lewicka-Szczebak et al., 2017) with a flow of 9 mL min^{-1}. Gas samples were collected daily into two 12 mL septum-capped Exetainers® (Labco Limited, Ceredigion, UK) and one crimped 100 mL vial connected to the vents of the incubation columns. Soil samples were collected five times during the incubation by sacrificing one incubation column per sampling event, which was then divided into three subsamples (replicate samples of mixed soil).

2.3 Gas analyses

Measurements of N_2O concentrations in the 20 mL samples were carried out with a gas chromatograph (GC-2014, Shimadzu, Duisburg, Germany) equipped with an electron capture detector (ECD) and an autosampler (Loftfields Analytical Solutions, Neu Eichenberg, Germany). The analytical precision was around 2 %.

Flux rates of total N_2O for field campaigns, i.e., including fluxes from ^{15}N-labeled and nonlabeled sources, were calculated from ordinary linear regression of the four consecutive samples over time using the R package gasfluxes (Fuß, 2015)

and the following equation:

$$J_{N_2O} = \frac{dC_{N_2O}}{dt} \times \frac{V}{A}, \quad (1)$$

where J_{N_2O} is the flux rate (in $\mu g\, N_2O\text{-}N\, m^{-2}\, h^{-1}$), C_{N_2O} is N_2O mass concentration (in $\mu g\, N\, m^{-3}$) corrected by the chamber temperature according to the ideal gas law, t is closing time of the chamber, V is volume of the chamber (in m^3), and A is covered soil area (in m^2).

For laboratory incubations, fluxes were calculated based on the dynamic chamber principle. Correction for the inlet concentration is omitted since the N_2O-free gas mixture was used for flushing:

$$J_{N_2O} = C_{N_2O} \times \frac{Q}{A}, \quad (2)$$

where J_{N_2O} is the flux rate (in $\mu g\, N_2O\text{-}N\, m^{-2}\, h^{-1}$), C is N_2O mass concentration (in $\mu g\, N\, m^{-3}$) corrected by the incubation temperature according to the ideal gas law, Q is the gas flow rate through the incubation vessels (in $m^3\, h^{-1}$), and A is soil area in the incubation vessel (in m^2).

The gas samples collected from ^{15}N treatments were analyzed for ^{15}N content with a modified GasBench II preparation system coupled to MAT 253 isotope ratio mass spectrometer (Thermo Scientific, Bremen, Germany) according to Lewicka-Szczebak et al. (2013). In this setup, N_2O is converted to N_2 during in-line reduction, and stable isotope ratios ^{29}R ($^{29}N_2/^{28}N_2$) and ^{30}R ($^{30}N_2/^{28}N_2$), of N_2, of the sum of denitrification products ($N_2 + N_2O$) and of N_2O are determined. Based on these measurements, the following values are calculated according to the respective equations (after Spott et al., 2006):

The ^{15}N abundance of the ^{15}N-labeled pool (a_P) from which N_2 ($a_{P\_N_2}$) or N_2O ($a_{P\_N_2O}$) originates is calculated as follows:

$$a_P = \frac{^{30}x_M - a_M \cdot a_{bgd}}{a_M - a_{bgd}}. \quad (3)$$

The calculation of a_P is based on the nonrandom distribution of N_2 and N_2O isotopologues (Spott et al., 2006), where $^{30}x_M$ is the fraction of $^{30}N_2$ in the total gas mixture,

$$^{30}x_M = \frac{^{30}R}{1 + {}^{29}R + {}^{30}R}; \quad (4)$$

a_M is ^{15}N abundance in total gas mixture,

$$a_M = \frac{^{29}R + 2\,{}^{30}R}{2(1 + {}^{29}R + {}^{30}R)}; \quad (5)$$

and a_{bgd} is ^{15}N abundance of the nonlabeled pool (atmospheric background or experimental matrix).

The fraction originating from the ^{15}N-labeled pool (f_P) for N_2 ($f_{P\_N_2}$), $N_2 + N_2O$ ($f_{P\_N_2+N_2O}$), and N_2O ($f_{P\_N_2O}$) within the total N of the sample is calculated as follows:

$$f_P = \frac{a_M - a_{bgd}}{a_P - a_{bgd}}. \quad (6)$$

The fraction originating from the ^{15}N-labeled pool within the sample (f_{N_2}) is calculated, taking into account the actual N_2 concentration background in the sample C_{N_2}:

$$f_{N_2} = f_{P\_N_2} \times C_{N_2}. \quad (7)$$

From the f_{N_2} value determined with Eq. (7), the N_2 flux was calculated, in the same manner as for N_2O, for field campaigns (Eq. 1):

$$J_{N_2} = \frac{f_{N_2}}{dt} \times \frac{V}{A}, \quad (8)$$

where J_{N_2} is the N_2 flux rate (in $\mu g\, N_2\text{-}N\, m^2\, h^{-1}$), f_{N_2} is N_2 mass concentration (in $\mu g\, N\, m^3$) corrected by the chamber temperature according to the ideal gas law, t is closing time of the chamber, V is volume of the chamber (in m^3), and A is covered soil area (in m^2). Chamber closing time was 120 min, and for one chosen field study (F3) the linearity of N_2 increase over 120 min was checked and confirmed. The flux correction for underestimation due to subsoil flux and gas soil storage (Well et al., 2019b) was not performed because the focus of this paper was to determine r_{N_2O}, while subsoil diffusion of N_2 and N_2O is almost identical. This correction would thus not significantly impact r_{N_2O}. But the fluxes shown in Fig. S2 in the Supplement are measured fluxes and include the underestimation of ^{15}N-based estimates (Well et al., 2019b).

For laboratory incubations with the constant flow through, N_2 flux was determined in the same manner as for N_2O (Eq. 2):

$$J_{N_2} = f_{N_2} \times \frac{Q}{A}, \quad (9)$$

where J_{N_2} is the N_2 flux rate (in $\mu g\, N_2\text{-}N\, m^{-2}\, h^{-1}$), $f_{P\_N_2}$ is N_2 mass concentration (in $\mu g\, N\ m^3$) corrected by the chamber temperature according to the ideal gas law, Q is the gas flow rate through the incubation vessels (in $m^3\, h^{-1}$), and A is soil area in the incubation vessel (in m^2).

N_2O residual fraction (r_{N_2O}) representing the unreduced N_2O mole fraction of total gross N_2O production (Lewicka-Szczebak et al., 2017) is calculated as

$$r_{N_2O} = \frac{J_{N_2O}}{J_{N_2O} + J_{N_2}}, \quad (10)$$

where J_{N_2O} and J_{N_2} are the N_2O and N_2 flux rates (in $\mu g\, N_2O\text{-}N\, m^{-2}\, h^{-1}$).

The analytical detection limit of the calculated N_2 flux from the ^{15}N-labeled pool was approx. $50\, \mu g\, N\, m^2\, h^{-1}$ for field studies and approx. $1.5\, \mu g\, N\, m^2\, h^{-1}$ for laboratory experiments (due to increased sensitivity as a result of the N_2-reduced atmosphere).

The gas samples collected in NA treatments were analyzed for isotopocule N_2O signatures using a Delta V isotope ratio mass spectrometer (Thermo Scientific, Bremen, Germany), which was coupled to an automatic preparation system with PreCon plus Trace GC IsoLink (Thermo Scientific); in this system, N_2O was preconcentrated, separated, and purified, and m/z 44, 45, and 46 of the intact N_2O^+ ions as well as m/z 30 and 31 of NO^+ fragment ions were determined. The results were evaluated accordingly (Röckmann et al., 2003; Toyoda and Yoshida, 1999; Westley et al., 2007), which allows for the determination of average $\delta^{15}N$, $\delta^{15}N^{\alpha}$, ($\delta^{15}N$ of the central N position of the N_2O molecule), and $\delta^{18}O$; $\delta^{15}N^{\beta}$ ($\delta^{15}N$ of the peripheral N position of the N_2O molecule) was calculated as $\delta^{15}N = (\delta^{15}N^{\alpha} + \delta^{15}N^{\beta})/2$, and ^{15}N site preference ($\delta^{15}N^{SP}$) as $\delta^{15}N^{SP} = \delta^{15}N^{\alpha} - \delta^{15}N^{\beta}$.

Pure N_2O analyzed for isotopocule values in the laboratory of the Tokyo Institute of Technology was used as internal reference gas by applying calibration procedures reported previously (Toyoda and Yoshida, 1999; Westley et al., 2007). Moreover, the standards from a laboratory intercomparison (REF1, REF2) were used for performing two-point calibration for $\delta^{15}N^{SP}$ values (Mohn et al., 2014). All isotopic values are expressed as per mill (‰) deviation from the $^{15}N/^{14}N$ and $^{18}O/^{16}O$ ratios of the reference materials (i.e., atmospheric N_2 and Vienna Standard Mean Ocean Water (VSMOW), respectively). The analytical precision determined as standard deviation (1σ) of the internal standards for measurements of $\delta^{15}N$, $\delta^{18}O$, and $\delta^{15}N^{SP}$ were typically 0.1 ‰, 0.1 ‰, and 0.5 ‰, respectively.

2.4 Soil analyses

All soil samples were homogenized. Soil water content was determined by weight loss after 24 h drying at 110 °C. Soil pH was determined in 0.01 M $CaCl_2$ solution (ratio 1 : 5). Nitrate and ammonium concentrations were determined by extraction in 2 M KCl in 1 : 4 ratio by 1 h shaking. Nitrite concentration was determined in alkaline extraction solution of 2 M KCl with addition of 2 M KOH (25 mL L^{-1}) in 1 : 1 ratio for 1 min of intensive shaking (Stevens and Laughlin, 1995). The amount of added KOH was adjusted to keep the alkaline conditions in extracts (pH over 8). After shaking, the samples were centrifuged for 5 min and filtrated. The extracts for NO_2^- measurements were stored at −4 °C and analyzed within 5 d. NO_3^-, NH_4^+, and NO_2^- concentrations were determined colorimetrically with an automated analyzer (Skalar Analytical B.V., Breda, the Netherlands).

To determine the isotopic signatures of mineral nitrogen in NA treatments, microbial analytical methods were applied. For nitrate, the bacterial denitrification method with *Pseudomonas aureofaciens* was applied (Casciotti et al., 2002; Sigman et al., 2001). For nitrite, the bacterial denitrification method for selective nitrite reduction with *Stenotrophomonas nitritireducens* was applied (Böhlke et al., 2007), as well as for ^{15}N-enriched samples from ^{15}N treatments. For ammonium, a chemical conversion to nitrite with hypobromite oxidation (Zhang et al., 2007) followed by bacterial conversion of nitrite after pH adjustment was applied (Felix et al., 2013).

In ^{15}N treatments, ^{15}N abundances of NO_3^- ($a_{NO_3^-}$) and NH_4^+ ($a_{NH_4^+}$) were measured according to the procedure described in Stange et al. (2007) and Eschenbach et al. (2017). NO_3^- was reduced to NO by vanadium-III chloride (VCl_3) and NH_4^+ was oxidized to N_2 by hypobromite (NaOBr). NO and N_2 were used as measurement gas. Measurements were performed with a quadrupole mass spectrometer (GAM 200, InProcess Instruments, Bremen, Germany).

2.5 N_2O isotope mapping approach (MAP)

The mapping approach is based on the different slopes of the mixing line between bD (possibly including also nD) and fD or Ni and the reduction line reflecting isotopic enrichment of residual N_2O due to its partial reduction in dual-isotope plots. Both lines are defined from the known most relevant literature data on the respective mixing endmember isotopic signatures and reduction fractionation factors. The detailed isotopic characteristics applied for the isotope MAPs are presented in Table 1 and follow the most recent review paper (Yu et al., 2020). The detailed calculation strategy for SP/O MAP can be found in the Supplement for the Wu et al. (2019) paper and for SP/N MAP in the Supplement for the Toyoda et al. (2011) paper. The calculations are performed according to two possible cases of N_2O mixing and reduction:

- Case 1 – N_2O produced from bD is first partially reduced to N_2, followed by mixing of the residual N_2O with N_2O from other pathways.
- Case 2 – N_2O produced by various pathways is first mixed and afterwards reduced.

The calculations can be performed following different scenarios of particular endmember mixing: either bD-fD mixing or bD-Ni mixing. For our case studies, due to rather high soil moisture (> 60 % WFPS) and low ammonium content (Table 2), we rather expect higher fD contribution than Ni; hence, the bD-fD mixing was applied and contribution of Ni was neglected. In the Supplement, we also present a comparison of calculation results based on both mixing scenarios bD-fD and bD-Ni (Table S1 and spreadsheet table in the Supplement). This comparison only showed pronounced differences for the F1 treatment. The bD fraction determined by this approach may also include the nD fraction, since nD cannot be separated from bD due to isotope overlap (Fig. 1).

For the graphical presentation of dual-isotope plots for sampling points, $\delta^{18}O$ and $\delta^{15}N$ values of emitted N_2O are always plotted ($\delta^{18}O_{N_2O}$, $\delta^{15}N_{N_2O}$). But the precursor isotopic signatures ($\delta^{18}O_{H_2O}$, $\delta^{15}N_{NO_3^-}$, $\delta^{15}N_{NH_4^+}$) are taken into account by respective correction of mixing endmember isotopic ranges (see Table 1). The literature endmember ranges are given as isotope effects (ε) expressed in relation

to particular precursors relevant for a particular pathway:

$$\varepsilon_{N_2O/precursor} = \delta_{N_2O} - \delta_{precursor}. \quad (11)$$

For example, for $\delta^{18}O$ of bD, the ε_{N_2O/H_2O} is calculated by subtracting the precursor isotopic signature (δ_{H_2O}) from the measured δ_{N_2O} values (i.e., $\delta_{N_2O} = 10$ and $\delta_{H_2O} = -9$, so $\varepsilon_{N_2O/H_2O} = 19$).

Afterwards, the literature isotope effects are corrected with the actually measured precursor values determined for the particular study ($\delta_{actual\ precursor}$) to determine the characteristic isotopic signature of N_2O emitted from the particular mixing endmember for these study conditions ($\delta_{N_2O,\ endmember}$):

$$\delta_{N_2O\_endmember} = \varepsilon_{N_2O/precursor} + \delta_{actual\ precursor}. \quad (12)$$

For example, for $\delta^{18}O$ of bD, $\varepsilon_{N_2O/H_2O} = 19$, $\delta_{actual\ H_2O} = -6.4$, and $\delta_{N_2O\_bD} = 12.6$.

Hence, the endmember ranges represent the expected isotopic signatures of N_2O originating from each mixing endmember for the particular case study characterized by specific precursor isotopic signatures. Such an approach allows for presenting all data in the common isotopic scales without presumption on the dominating pathway and dominating precursor. Hence, this new approach presented here is actually a further development of MAPs, since this allows for correcting both Ni/nD and bD/fD endmembers with relevant distinct precursors, in contrast to only correcting measured values with one common assumed precursor isotopic signature. In previous papers, where $\delta^{18}O$ and $\delta^{15}N$ related to precursors ($\delta^{18}O_{N_2O/H_2O}$, $\delta^{15}N_{N_2O/NO_3}$) were plotted (Ibraim et al., 2019; Lewicka-Szczebak et al., 2017, 2016), it was assumed that denitrification must be the dominating N_2O production pathway.

2.6 Three-dimensional N_2O isotopocule model (3DIM)

The probability distributions of proportional contributions f_i were determined using a stable isotope mixing model in the Bayesian framework. This allowed us to integrate three N_2O isotopic signatures into one model to find the nearest solution for the r_{N_2O} and mixing proportions. The core of the model was based on the work of Moore and Semmens (2008), which was further extended with implementation of N_2O reduction in two possible cases (analogically as for MAPs – see Sect. 2.5).

$$\text{Case 1}: f_{bD}(\delta_{bD} + \varepsilon \ln(r_{bD})) + f_{nD}\delta_{nD} + f_{fD}\delta_{fD} + f_{Ni}\delta_{Ni} = \delta_{N_2O}, \quad (13)$$

$$\text{Case 2}: f_{bD}\delta_{bD} + f_{nD}\delta_{nD} + f_{fD}\delta_{fD} + f_{Ni}\delta_{Ni} + \varepsilon \ln(r_{N_2O}) = \delta_{N_2O}, \quad (14)$$

where f stands for fraction of N_2O originating from a particular pathway and δ stands for isotopic signature characteristic of this pathway for bD, nD, fD, and nitrification Ni; ε is the isotope fractionation factor for N_2O reduction to N_2, and r_{N_2O} is the N_2O residual fraction as defined in Eq. (10); r_{bD} is the N_2O residual fraction of bacterial denitrification only, as it is assumed in Case 1. This value can be recalculated to obtain r_{N_2O} as follows:

$$r_{N_2O} = f_{bD}r_{bD} + f_{nD} + f_{fD} + f_{Ni}. \quad (15)$$

Let us briefly summarize the key assumptions and features of the statistical model. The input data of measured m isotope signatures (here three: $\delta^{15}N$, $\delta^{15}N^{SP}$, $\delta^{18}O$) from n sources (here four: bD, nD, fD, and Ni) are assumed to be normally distributed, and multiple measurements (here one to seven replicates) constitute a single sample, on which the Monte Carlo integration is performed. The uncertainties in the source data are fed into the model through the variance in the calculation of unnormalized likelihood (see Eq. 18). For prior distributions of parameters, a flat Dirichlet distribution was used for proportional source contributions f_i and uniform distribution for reduction parameter r. For each random sample (f_i, r), a mean and a variance of each isotope signature j are calculated (different for two cases listed above):

$$\text{Case 1}: \quad \mu_j = \sum_{i=1}^{n}(f_i\delta_{ij}) + f_{bD}\varepsilon \ln(r_{bD})\sigma_j = \sqrt{\sum_{i=1}^{n}(f_i\sigma_{ij}^2) + f_{bD}|\ln(r_{bD})|\sigma_{\varepsilon j}^2}, \quad (16)$$

$$\text{Case 2}: \quad \mu_j = \sum_{i=1}^{n}(f_i\delta_{ij}) + \varepsilon \ln(r_{N_2O})\sigma_j = \sqrt{\sum_{i=1}^{n}(f_i\sigma_{ij}^2) + |\ln(r_{N_2O})|\sigma_{\varepsilon j}^2}, \quad (17)$$

and the likelihood of such a combination is calculated as

$$L(x|\mu_j, \sigma_j) = \prod_k^N \prod_j^m \left[\frac{1}{\sigma_j\sqrt{2\pi}} \exp\left(\frac{-(x_{kj} - \mu_j)^2}{2\sigma_j^2}\right)\right], \quad (18)$$

where x_{kj} stands for kth measurement of the sample and jth isotope signature. We use the Markov-chain Monte Carlo method with the Metropolis condition: $L_{i+1}/L_i \geq \alpha$, where α is a random variable sampled from a uniform distribution.

The detailed input parameters for the model are presented in Table 1. The detailed isotopic characteristics to be applied for the isotope signatures of mixing endmembers and reduction fractionation factors are adopted after the most recent review paper (Yu et al., 2020).

2.7 Statistics

For results comparisons, an analysis of variance was used with the significance level α of 0.1. The uncertainty values provided for the measured parameters represent the standard deviation (1σ) of the replicates. The propagated uncertainty was calculated using the Gauss error propagation equation, taking into account standard deviations of all individual parameters.

The agreement with the reference method was assessed with the Nash–Sutcliffe efficiency (F) (Nash and Sutcliffe, 1970), which represents the R of the fit to the 1 : 1 line between observed reference (O) and estimated (E) values, as

Table 1. Summary of mixing endmember isotopic signatures of particular pathways (bD – bacterial denitrification, nD – nitrifier denitrification, fD – fungal denitrification, Ni – nitrification) and reduction fractionation factors (reduction) with respective references. For the model input, each value is corrected with the respective mean isotopic signature of the substrate: for $\delta^{18}O$ – soil water ($\delta^{18}O_{H_2O}$) for bD, nD, and fD; for $\delta^{15}N$ – respective substrate – NO_3^- for bD and fD; and for NH_4^+ for nD and Ni, with distinct values applied for field ($\delta^{15}N_{field}$ for F1, F2, and F3) and laboratory ($\delta^{15}N_{lab}$ for L1, L2) studies. The respective substrate-corrected values were applied as a model input for $\delta^{18}O$ and $\delta^{15}N$; for $\delta^{15}N^{SP}$ no substrate correction is needed. The final model input values are marked with bold font.

	Literature values			Substrate isotope values			Substrate-corrected values		
Pathway	$\delta^{15}N^{SP}$	$\varepsilon^{18}O$	$\varepsilon^{15}N$	$\delta^{18}O_{H_2O}$	$\delta^{15}N_{field}$	$\delta^{15}N_{lab}$	$\delta^{18}O$	$\delta^{15}N_{field}$	$\delta^{15}N_{lab}$
bD[a]	**−1.9 ± 4.6**	19.0 ± 2.1	−45.8 ± 4.7	−6.4	11.9	4.5	**12.6 ± 2.1**	**−33.9 ± 4.7**	**−41.3 ± 4.7**
nD[b]	**−5.9 ± 6.5**	15.7 ± 2.9	−56.9 ± 3.8	−6.4	41.4	79.3	**9.3 ± 2.9**	**−15.5 ± 3.8**	**22.4 ± 3.8**
fD[c]	**33.6 ± 2.5**	46.9 ± 3.8	−38.0 ± 6.6	−6.4	11.9	4.5	**40.5 ± 3.8**	**−26.1 ± 6.6**	**−33.5 ± 6.6**
Ni[d]	**35.0 ± 2.9**	**23.5 ± 2.1**	−57.0 ± 7.3		41.4	79.3		**−15.6 ± 7.3**	**22.3 ± 7.3**
Reduction[e]	**−6.0 ± 1.4**	**−15.9 ± 4.7**	**−7.0 ± 2.1**						

[a] Barford et al. (1999); Lewicka-Szczebak et al. (2016, 2014); Rohe et al. (2017); Sutka et al. (2006); Toyoda et al. (2005). [b] Frame and Casciotti (2010); Sutka et al. (2006). [c] Maeda et al. (2015); Rohe et al. (2014a, 2017); Sutka et al. (2008). [d] Frame and Casciotti (2010); Mandernack et al. (2009); Sutka et al. (2006); Yoshida (1988). [e] Jinuntuya-Nortman et al. (2008); Lewicka-Szczebak et al. (2015, 2014); Menyailo and Hungate (2006); Ostrom et al. (2007); Well and Flessa (2009).

also used in previous validation studies (Lewicka-Szczebak et al., 2017; Wu et al., 2019):

$$F = 1 - \frac{\sum_{i=1}^{n}(O_i - E_i)^2}{\sum_{i=1}^{n}(O_i - O)^2}, \quad (19)$$

where E_i is the r_{N_2O} value estimated with the method under validation, corresponding to the observed r_{N_2O} value determined with the reference method (O_i), and O is the observed mean. In this assessment, an $F = 1$ refers to a perfect fit between estimated and reference values, lower F values indicate worse model fits, and a negative F occurs when the observed mean is a better predictor than the model.

3 Results

3.1 Soil properties

Soil organic N was analyzed in soil samples from each sampling campaign and varied only slightly with content of 0.141 % ± 0.007 % N and isotopic signature $\delta^{15}N$ of 7.4 ‰ ± 0.4 ‰. $\delta^{18}O$ of soil water varied only slightly for field campaigns and equaled −6.7 ‰ for F1, −7.0 ‰ for F2, and −6.4 ‰ for F3, but was higher for incubation experiments with mean of −5.3 ‰. Detailed characteristics for mineral nitrogen contents and isotopic signatures are presented in Table 2. The variations in water and nitrate content during the field campaigns and laboratory incubations with comparison between NA and ^{15}N treatment are presented in the Supplement (Fig. S1). Importantly, for the vast majority of sampling points these soil conditions are well comparable between both treatments, which allows for the comparison of the methods. Significant difference was only noted for nitrate content for the last sample in L2 and for water content for the last sample in F1 (Fig. S1).

3.2 Field campaigns

The first field campaign (F1) in November 2015 (23–27 November) showed low N_2O fluxes from 1.2 to 33.2 g N-N_2O ha^{-1} d^{-1} (Table 2). N_2O isotopic signatures were determined for all the samples except one. The N_2 fluxes were under the detection limit for all samples, i.e., below 11 g N-N_2 ha^{-1} d^{-1}. In this case, the reference r_{N_2O} values from the ^{15}N treatment could not be precisely determined. However, from the information that N_2 flux is below the detection limit even for the highest N_2O fluxes observed, we can assess that r_{N_2O} must be higher than 0.75. For F1, soil temperature varied from 1.6 to 8.6 °C (mean 4.1 °C); WFPS varied from 54.1 to 72.4 % (mean 65 %).

The second field campaign (F2) in March 2016 (7–11 March) showed very variable N_2O fluxes from 0.5 to 110.7 g N-N_2O ha^{-1} d^{-1}. N_2O isotopic signatures could be determined only in 17 samples from 26. The N_2 fluxes were above the detection limit for 15 samples from 26, and they varied from 23 to 304 g N-N_2 ha^{-1} d^{-1}. In this case, the reference r_{N_2O} values from the ^{15}N treatment could be determined for four sampling dates out of eight. For F2, soil temperature varied from 1.4 to 12.0 °C (mean 6.4 °C); WFPS varied from 57.9 to 77.9 % (mean 69 %).

The third field campaign (F3) in May/June 2016 (30 May–3 June) showed very high N_2O fluxes from 1 to 1471 g N-N_2O ha^{-1} d^{-1}. N_2O isotopic signatures could be determined in all samples. The N_2 fluxes were always above the detection limit and varied from 114 to 2060 g N-N_2 ha^{-1} d^{-1}. In this case, the reference r_{N_2O} values from the ^{15}N treatment could be determined for all eight sampling times. For F3, soil temperature varied from 17.0 to 32.5 °C (mean 21.4 °C); WFPS varied from 52.1 % to 72.0 % (mean 62 %).

The detailed variations in gas fluxes during field campaigns, variations in ^{15}N abundance in various pools (a_{NO_3},

$a_{P\_N_2O}$, and $a_{P\_N_2}$), and the N_2O ^{15}N-pool-derived fraction ($f_{P\_N_2O}$) are presented in the Supplement (Figs. S2c–e and S3c–e). There are no significant differences in N_2O flux between ^{15}N and NA treatment (Fig. S2c–e). In F3 the fluxes were much larger than in F1 and F2 and were decreasing during the sampling campaign, whereas N_2 flux was very variable and showed large differences between repetitions, represented by large error bars (Fig. S2e). In F1 and F2, the ^{15}N-pool-derived fraction was significantly lower when compared to F3. In F3, $a_{P\_N_2}$ and $a_{P\_N_2O}$ were comparable and higher than a_{NO_3} in the first three samples and similar with a_{NO_3} for the last five samples. In F2, $a_{P\_N_2O}$ strictly depended on a_{NO_3}, and both showed clear decreasing trends, whereas $a_{P\_N_2}$ was determined only in two sampling points and was significantly lower than $a_{P\_N_2O}$ and a_{NO_3}.

3.3 Laboratory experiments

The laboratory experiment L1 was conducted in dryer conditions than L2. In L1 initially WFPS was about 60 %, and after water addition (9th day of the experiment) it was increased to 65 %. In L2 initially WFPS was about 70 %, and after water addition (9th day of the experiment) it was increased to 80 %. N_2O fluxes in L1 were quite low: from 0.2 to 16.7 g N-N_2O ha^{-1} d^{-1}. N_2O isotopic signatures could be determined in 38 out of 56 samples. The N_2 fluxes were above the detection limit only for 43 out of 112 samples and varied from 1.5 to 69.4 g N-N_2 ha^{-1} d^{-1}. In this case the reference r_{N_2O} values from the ^{15}N treatment could only be determined for 7 sampling times out of 10. In L2 N_2O fluxes were higher and varied in a wide range from 0.4 to 297.4 g N-N_2O ha^{-1} d^{-1}. N_2O isotopic signatures could be determined in 40 out of 56 samples. The N_2 fluxes were above the detection limit only for 87 out of 112 samples and varied from 1.2 to 199 g N-N_2 ha^{-1} d^{-1}. In this case, the reference r_{N_2O} values from the ^{15}N treatment could be determined for 9 sampling times out of 10.

The detailed variations in gas fluxes during laboratory incubations, variations in ^{15}N abundance in various pools (a_{NO_3}, $a_{P\_N_2O}$, and $a_{P\_N_2}$), and the N_2O ^{15}N-pool-derived fraction ($f_{P\_N_2O}$) are presented in the Supplement (Figs. S2a, b and S3a, b). We often observe significantly different fluxes for NA and ^{15}N treatment: for L1 only for two samples (4 and 5) NA treatment showed significantly higher N_2O flux, but for L2 the majority of sampling points shows a significantly higher N_2O flux in the ^{15}N treatment, particularly for the last four sampling points, after the water addition (Fig. S2b). Importantly, water content did not differ for these sampling points. In L1 the ^{15}N-pool-derived fraction was significantly lower when compared to L2. In both L1 and L2, $a_{P\_N_2}$, $a_{P\_N_2O}$, and a_{NO_3} showed comparable ranges and only a very slight decreasing trend (Fig. S3a, b).

3.4 MAPs

O / SP MAP

The majority of isotope results presented in the SP/O MAP (Fig. 1) is situated within the area limited by reduction and mixing lines, which allows for application of the calculation approach based on SP/O MAP. Numerous samples, mostly from the laboratory incubation studies, are situated below the mean reduction line but within the minimum reduction line. For these samples, the calculation results provide f_{bD} values slightly above 1, which are set to 1 for the further summaries. All calculations and results can be followed in the spreadsheet file in the Supplement.

The endmember isotope values applied here (after Yu et al., 2020) differ for nitrification $\delta^{18}O$ when compared to previous applications of SP/O MAP (Buchen et al., 2018; Ibraim et al., 2019; Lewicka-Szczebak et al., 2017; Verhoeven et al., 2019). The currently applied $\delta^{18}O$ endmember values for Ni (23.5 ‰ ± 2.1 ‰) are lower than the previously applied range (from 38.0 ‰ to 55.2 ‰, mean 43.0 ‰) and thus result in a separation of Ni and fD, which was not possible in the previous studies. With the current values, we have two possible mixing lines (bD-Ni and bD-fD), whereas in previous studies only one mixing line was applied (bD − (Ni + fD)). This requires the choice of the most appropriate mixing scenario for the particular case study. For this study, the results obtained for r_{N_2O} and f_{bD} differ (mostly) only very slightly for both mixing scenarios (see Table S1 and spreadsheet file in the Supplement), which is due to high f_{bD}. For F3, where f_{bD} is near 1, the difference in r_{N_2O} does not exceed 0.02, and for F1 with the lowest f_{bD} of ca. 0.7, the difference in r_{N_2O} reaches 0.22 (Table S1). Below we summarize the results of calculations assuming the bD-fD mixing scenario only.

The calculation has been performed with two cases (see Sect. 2.5), and all results are shown and compared with reference method in Tables 3 and 4. Due to quite high f_{bD} for our study, both cases show only very slight differences (Tables 3 and 4). For the field study F1, we obtained the highest r_{N_2O} values (0.86 ± 0.12) and the lowest f_{bD} values (0.74 ± 0.07). For field study F2, the r_{N_2O} values were lower (0.38 ± 0.05) and the f_{bD} values were higher (0.92 ± 0.04). For field study F3, the r_{N_2O} values were very similar as in F2 (0.33 ± 0.07) and the highest f_{bD} values were noted (0.99 ± 0.01). For the laboratory incubation studies, we obtained slightly lower ($p = 0.086$) r_{N_2O} for L1 (0.19 ± 0.03) when compared to L2 (0.27 ± 0.12). Both laboratory treatments showed very high f_{bD} for L1 (0.99 ± 0.01) and L2 (0.98 ± 0.04).

N / SP MAP

For the SP/N MAP, we present the literature endmember values in relation to the respective precursor, i.e., NO_3^- for bD and fD and NH_4^+ for nD and Ni (Table 1). For the field and

Table 2. Results summary.

	Treatment	F1	F2	F3	L1	L2
WFPS (%)		65.1 ± 4.3	69.1 ± 4.5	62.4 ± 4.1	60→65	70→80
N_2O flux	NA	8.9 ± 7.4	16.3 ± 26.1	331.3 ± 302.9	4.9 ± 4.7	8.5 ± 5.6
(g N-N_2O ha^{-1} d^{-1})	^{15}N	5.9 ± 5.5	4.3 ± 3.3	330.9 ± 323.7	1.4 ± 1.0	54.6 ± 50.2
N_2 flux[a](g N-N_2 ha^{-1} d^{-1})	^{15}N	bd (< 11.3)	108.2 ± 84.1[b]	576.4 ± 285.4	26.6 ± 18.1	45.3 ± 44.5
$r^{a}_{N_2O}$	^{15}N	nd (> 0.75)	0.06 ± 0.04[b]	0.33 ± 0.15	0.12 ± 0.10	0.49 ± 0.31
NO_3 content	NA	13.6 ± 3.1	8.0 ± 2.4	13.6 ± 3.2	21.2 ± 1.5	21.0 ± 1.7
(mg N per kg soil)	^{15}N	15.8 ± 6.2	7.5 ± 1.1	15.8 ± 5.5	20.1 ± 0.6	19.4 ± 1.1
NH_4 content	NA	3.8 ± 2.1	6.4 ± 3.3	3.4 ± 1.5	0.53 ± 0.19	0.71 ± 0.23
(mg N per kg soil)	^{15}N	2.0 ± 2.6	5.4 ± 3.1	3.7 ± 1.9	0.58 ± 0.2	0.72 ± 0.15
$\delta^{15}N_{NO_3}$ (‰)	NA	8.0 ± 5.4	11.7 ± 5.3	12.1 ± 3.7	4.5 ± 0.4	4.7 ± 0.55
$\delta^{15}N_{NH_4}$ (‰)	NA	31.0 ± 8.7	40.5 ± 6.8	42.2 ± 9.1	90.0 ± 7.9	70.4 ± 17.9
$a^{15}N_{NO_3}$ (at. %)	^{15}N	20.5 ± 9.6	40.3 ± 10.1	19.7 ± 5.8	13.6 ± 0.7	13.9 ± 0.8
$a^{15}N_{NH_4}$ (at. %)	^{15}N	0.7 ± 0.6	0.9 ± 0.4	0.5 ± 0.2	0.5 ± 0.03	0.5 ± 0.01
$a^{15}N_{NO_2}$ (at. %)	^{15}N	15.5 ± 9.4	21.9 ± 8.0	10.9 ± 2.3	8.5 ± 6.1	10.3 ± 3.8
$\delta^{15}N_{N_2O}$	NA	−33.4 ± 9.5	−20.2 ± 16.0	−14.0 ± 14.8	−2.4 ± 8.0	−17.7 ± 11.9
$\delta^{18}O_{N_2O}$	NA	22.7 ± 4.3	33.2 ± 5.6	33.4 ± 6.1	40.8 ± 5.5	36.8 ± 5.2
$\delta^{15}N^{SP}_{N_2O}$	NA	9.4 ± 4.5	11.6 ± 5.4	6.9 ± 5.2	9.0 ± 6.2	8.6 ± 3.1
$a^{15}N_{N_2O}$ (at. %)	^{15}N	7.5 ± 2.7	11.7 ± 7.3	16.2 ± 10.6	11.8 ± 0.72	13.7 ± 0.67
$f_{P\_N_2O}$	^{15}N	0.28 ± 0.12	0.23 ± 0.13	0.59 ± 0.19	0.69 ± 0.06	0.96 ± 0.09
$a_{P\_N_2O}$	^{15}N	0.28 ± 0.07	0.47 ± 0.09	0.26 ± 0.11	0.17 ± 0.02	0.15 ± 0.01
$a_{P\_N_2}$	^{15}N	nd	0.23 ± 0.11	0.33 ± 0.11	0.21 ± 0.07	0.18 ± 0.06

[a] determined in ^{15}N treatments with gas-flux method
[b] half of data below detection limit
bd – below detection limit
nd – not determined, due to N_2 flux below detection limit

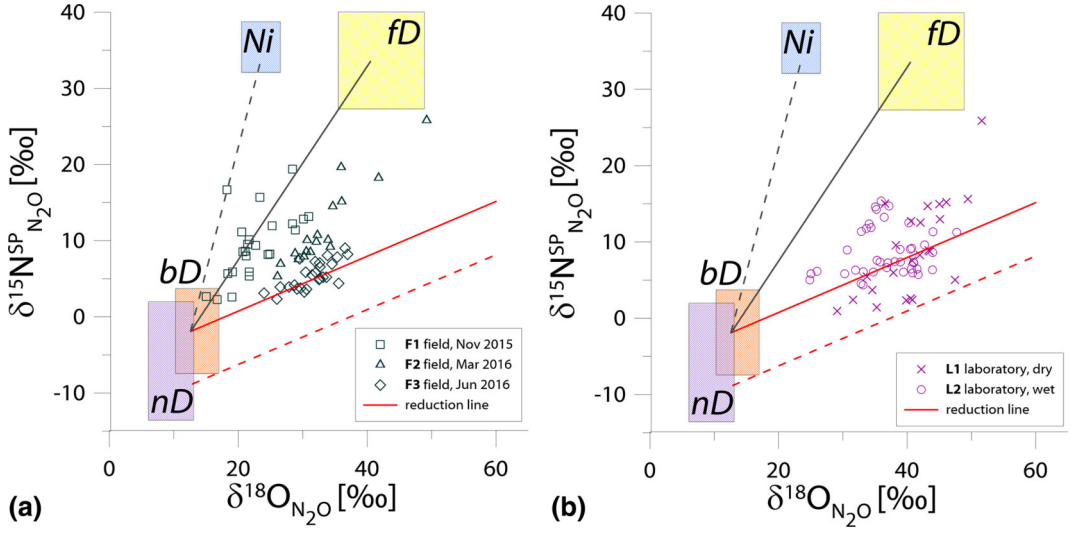

Figure 1. N_2O isotope data of field (**a**, green points) and laboratory studies (**b**, purple points) in SP/O MAP presented with literature endmember values and theoretical mixing (grey line) and reduction (red line) lines. The solid lines (bD-fD mixing and mean reduction line) are main assumptions used in the calculation procedures for SP/O MAP. The dashed grey line shows the alternative bD-Ni mixing line (calculations with this alternative scenario are also presented in Table S1 in the Supplement). The dashed red line shows the minimum reduction line – for the case of minimal delta values of the bD endmember. $\delta^{18}O$ values of mixing endmember bD, nD, and fD are presented in relation to the mean measured ambient water of −6.4 ‰ (hence present the expected $\delta^{18}O_{N_2O}$ originating from a particular pathway in these study conditions).

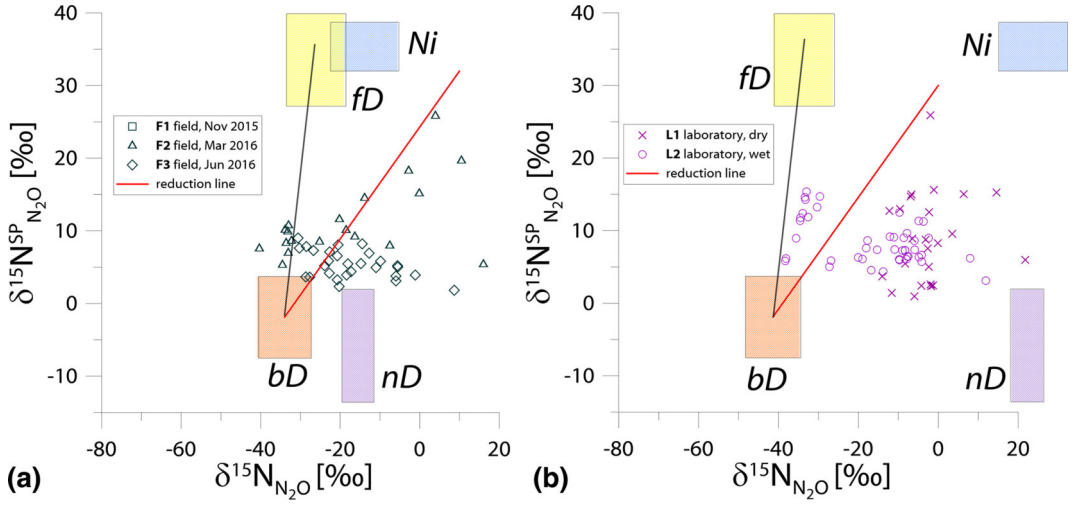

Figure 2. N_2O isotope data of field (green points) and laboratory (purple points) in SP/N MAP presented with literature mixing endmember values and theoretical mixing (grey line) and reduction (red line) lines. $\delta^{15}N$ values of mixing endmembers are presented in relation to the $\delta^{15}N$ of precursors: soil nitrate for bD and fD or ammonium for nD and Ni (hence present the expected $\delta^{15}N_{N_2O}$ originating from a particular pathway in these study conditions).

laboratory studies, separate mean values for NO_3^- (11.9 ‰ and 4.5 ‰, respectively) and NH_4^+ (41.4 ‰ and 79.3 ‰, respectively) were applied. These precursor isotopic signatures are the means of five samplings for each campaign and experiment. The extremely ^{15}N-enriched $\delta^{15}N_{NH_4}$ values result in a large shift of endmember ranges for nD and Ni. These ranges are ^{15}N-depleted in relation to bD when assuming identical $\delta^{15}N$ values for NO_3^- and NH_4^+, according to most previous studies (Ibraim et al., 2019; Koba et al., 2009; Toyoda et al., 2011). But in the case of our experiments, conversely, N_2O originating from nD and Ni would be significantly enriched in ^{15}N when compared to bD and fD (Fig. 2). For the samples, the measured bulk $\delta^{15}N_{N_2O}$ is plotted.

The majority of the samples is located outside the area limited by reduction and bD-fD mixing lines, which mostly precludes the application of the calculation approach based on SP/N MAP. The separation of mixing and reduction processes is not possible based on this plot, since the slopes of reduction line and bD-Ni mixing line are too similar, especially for laboratory experiments (Fig. 2b).

Another approach to include N precursor values is to apply the individual endmember isotopic signatures for each N_2O sample by interpolating the measured isotopic signatures of NO_3^- and NH_4^+. With five measurements of mineral N isotopic signatures per experiment, we get quite a good resolution for these values. Since they show quite high variations (Table 2), applying individual values is a better approach. But still (also by this approach), the majority of samples show values out of the calculation range, and the results are very ambiguous, representing the whole range of possible variations in both r_{N_2O} and f_{bD} values. Therefore these values are not summarized here.

O / N MAP

For O/N MAP (Fig. 3), the $\delta^{18}O$ values for bD, fD, and nD are expressed in relation to soil water; the $\delta^{15}N$ values for bD and fD are expressed in relation to soil NO_3^- and for nD and Ni in relation to soil NH_4^+ (Table 1). For these graphs, it is difficult to determine the reduction-mixing area because the slope of the reduction line is almost identical to the bD-fD mixing line.

A significant linear correlation has been found for both the field and laboratory studies, with $R^2 = 0.27$ ($p < 0.1$) and $R^2 = 0.40$ ($p < 0.01$), respectively. Both correlations show similar linear equations: $\delta^{18}O = 0.24 \times \delta^{15}N + 33.3$ and $\delta^{18}O = 0.28 \times \delta^{15}N + 41.6$ for field and laboratory studies, respectively (Fig. 3).

3.5 3DIM

The application of MAPs applying $\delta^{15}N$ data, i.e., SP/N MAP and O/N MAP, is very imprecise for this case study due to untypically high $\delta^{15}N_{NH_4}$ values and shifted location of the nD and Ni mixing endmembers (Figs. 2 and 3) when compared to cases when similar $\delta^{15}N_{NH_4}$ and $\delta^{15}N_{NO_3}$ values are determined or assumed. However, still the $\delta^{15}N$ data comprise important information, which can assist in process identification when applied jointly with the SP/O MAP. Therefore, we combined all the information into one 3DIM where all three isotopic signatures are taken into account.

The results of this model regarding r_{N_2O} are mostly well comparable to the values obtained with SP/O MAP (Ta-

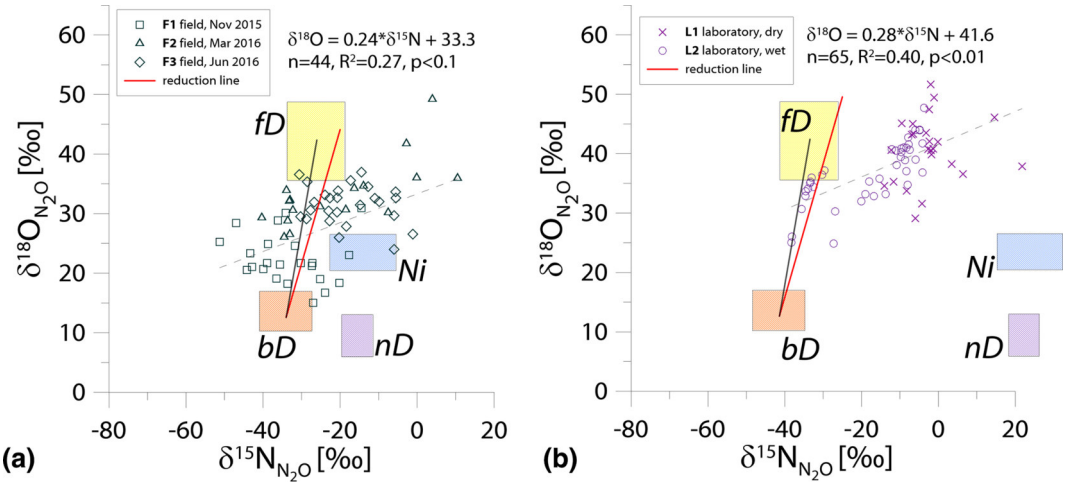

Figure 3. N_2O isotope data of field (**a**, green points) and laboratory (**b**, purple points) in O/N MAP presented with literature mixing endmember values and theoretical mixing (grey line) and reduction (red line) lines. $\delta^{15}N$ values are presented in relation to the $\delta^{15}N$ of precursors: soil nitrate for bD and fD or ammonium for nD and Ni. $\delta^{18}O$ values of mixing endmember bD, nD, and fD are presented in relation to the mean measured ambient water of −6.4 ‰. Hence, the mixing endmember ranges present the expected $\delta^{15}N_{N_2O}$ and $\delta^{18}O_{N_2O}$ originating from a particular pathway in these study conditions. The dashed line shows the linear fit for all the points with its equation and statistics above.

ble 3). However, for SP/O MAP both Case 1 and Case 2 provide similar results for r_{N_2O}, whereas for 3DIM these differ more pronouncedly. With the bar plots (Fig. 4) we summarize the results obtained from both modeling cases and below we summarize the results of Case 2, which provides more reliable results, as further discussed (see Sect. 4.2).

We get a much more detailed estimation regarding mixing proportions with 3DIM when compared to the SP/O MAP. The dominating N_2O production pathway is clearly bD, which contributes to N_2O production from 46 % for F2 up to 69 % for L2 (Fig. 4). An important role is also played by nD by contributing from 15% for L2 up to 40% N_2O for F3; low f_{nD} of 4 % was found for F1. The f_{fD} is quite variable from 6 % for F3 to 26 % for F1. Ni shows the lowest contribution around 3 %–5 %, and only a slightly higher f_{Ni} of 13 % was found for F2 (Fig. 4). N_2 fluxes are highly variable between the experiments, i.e., mean r_{N_2O} values vary from 0.21 for L1 to 0.89 for F1 (Fig. 4, Table 3).

The model provides very detailed information on probability distribution of the results, which is presented on the matrix plots prepared after Parnell et al. (2013) (Fig. S4 in the Supplement), where histograms of probability distribution of r_{N_2O} and mixing proportions, correlations between the modeled fractions, and R coefficients of these correlations are presented (Fig. S4). This summary provides an overview of the reliability of the model outputs and allows for identifying unavoidable model inadequacy. For all the modeled random samples, we observe very strong negative correlation between f_{bD} and f_{nD}, similar for both cases, from −0.28 to −0.93 (mean −0.63) and between f_{bD} and f_{fD} from −0.15 to −0.97 (mean −0.74); r_{N_2O} for Case 2 is always correlated negatively with f_{bD} from −0.15 to −0.84 (mean −0.62) and positively with f_{fD} from 0.18 to 0.82 (mean 0.62). For Case 1, this correlation is extremely variable for r_{N_2O}/f_{bD} from −0.67 to 0.85 and for r_{N_2O}/f_{fD} from −0.72 to 0.69. The lowest correlation coefficients are noted for f_{Ni}, where mean values never exceed 0.4. This is reflected in the determined ranges of possible results presented in the histograms. The f_{Ni} range is typically much narrower than f_{bD} and f_{nD} ranges.

The correlations and histograms vary between the particular campaigns with some typical features. For F1, we observe a very similar output for Case 1 and Case 2, quite narrow ranges of results, and no extremely high correlations. For F2, the ranges are much larger and high negative correlations for f_{bD}/f_{nD} and f_{fD}/f_{Ni} indicate possible imprecision in separation of these pathways, which results in a much wider range of probable results. For F3, the most extreme negative correlation for f_{bD}/f_{nD} is noted, and for Case 1 also r and f_{nD} show very strong correlation, which may affect the proper estimation of r_{N_2O}. For L1 and L2, we observe lower correlation f_{bD}/f_{nD} but higher f_{bD}/f_{fD}, which is probably a result of different $\delta^{15}N$ endmember values for nD and Ni and better separation of these pathways. The strong positive correlation of r_{N_2O} and f_{bD} for Case 1 in L1, F2, and F3 is rather a logical consequence of the assumptions underlying the Case 1 approach.

3.6 Comparison of r_{N_2O} with independent estimates

The N_2O reduction progress calculated with the above-presented SP/O MAP and 3DIM were compared with the results from the ^{15}N gas-flux method. In the tables below

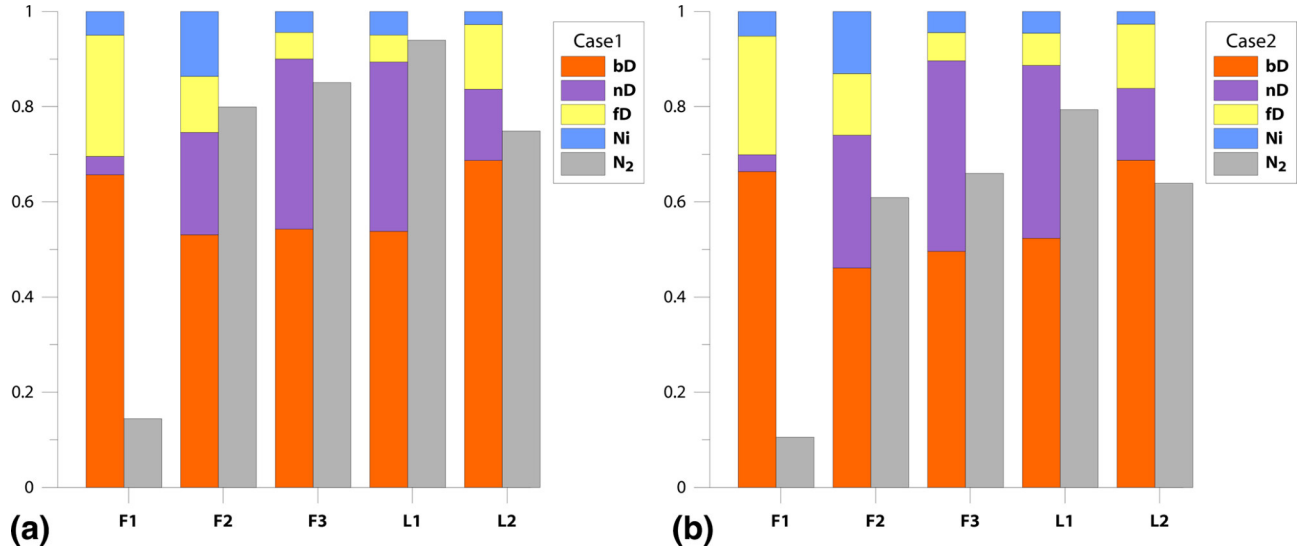

Figure 4. Bar plots showing modeled pathway fractions (f_{bD}, f_{nD}, f_{fD}, f_{Ni}) and N_2 flux contribution in the total (N_2+N_2O) flux ($1-r_{N_2O,}$). Results for both modeling cases, Case 1 **(a)** and Case 2 **(b)**, are shown.

we present the detailed comparison with the results applying both calculation cases (Case 1 and Case 2) for r_{N_2O} (Table 3) and for mixing proportions (Table 4).

The ranges and the mean values of the replicate means of all sampling dates are well comparable for SP/O MAP and 3DIM Case 2. Most inconsistent results are obtained in Case 1 of 3DIM; however, for L2 this case seems to be most accurate.

Since the variations of r_{N_2O} values in the experiments are very variable in time, just a comparison of overall mean values is not informative; we need to compare the temporal changes in r_{N_2O} (Fig. 5).

Most extreme changes in time are reported for the laboratory experiment L2 where a very sudden change in r_{N_2O} was observed as a consequence of water addition (between sampling 5 and 6). All three estimates present the same trend as the reference method, however, with lower amplitude of the temporal change (Fig. 5b). For field study F3, ^{15}N treatment indicates a constant decrease in r_{N_2O}, which is only partially reflected in SP/O MAP and not at all in 3DIM results. F1 and F2 data are not complete due to N_2 fluxes under detection limit for the whole F1 sampling and half of the samples of F2 campaign. However, for this missing data we can make estimates of the r_{N_2O} based on the known detection limit for N_2 flux. We estimated the r_{N_2O} values for the missing points assuming the possible N_2 flux: from 0 up to the detection limit of 11.3 g N-N_2 ha^{-1} d^{-1}.

In Fig. 6 we checked the fit of r_{N_2O} values determined by ^{15}N gas-flux method and 3DIM (Fig. 6a) or SP/O MAP (Fig. 6b). When analyzing all the individual sampling dates or all experiments, the fit to the 1 : 1 line is not very good, especially for many dates of the L2 experiment r_{N_2O} is largely underestimated with isotopocule approaches. This is mostly due to the sudden change in r_{N_2O} as presented above (Fig. 5b). But when we compare the means of the whole experiment or the experimental phases before and after water addition for L1 and L2 (red points in Fig. 6), the fit is much better with all points within the error of 0.15 for 3DIM. For SP/O MAP, the L2 mean after irrigation still shows larger disagreement.

The agreement between isotopocule methods and the reference method was statistically checked with F value (Eq. 19). The results for all means, minima, and maxima are shown in Table 3. The statistically significant agreement was indicated for SP/O MAP ($p < 0.1$) and Case 2 of 3DIM ($p < 0.05$), whereas Case 1 of 3DIM shows no agreement. Particular F values calculated with all sampling date means indicate no significant agreement ($F = 0.13$ for F3, $F = 0.45$ for L1, $F = 0.28$ for L2 – values for fit between Case 2 of 3DIM and reference method), which reinforces the observation, based on Fig. 6, that only mean experimental values show good agreement with the reference method but not the individual samplings.

3.7 Comparison of mixing proportions with independent estimates

The mixing proportions obtained by different approaches are much more complex to compare than r_{N_2O} due to the fact that each approach provides distinct information.

– With the reference method – ^{15}N gas flux – we determine the ^{15}N-pool-derived fraction of N_2O ($f_{P\_N_2O}$); hence, for the $^{15}NO_3$ treatment this is the fraction of N_2O originating from the labeled $^{15}NO_3$ pool. Theoretically, this can be bD or fD. It was intended to use the $^{15}NH_4^+$ treatment for the determination of N_2O fraction

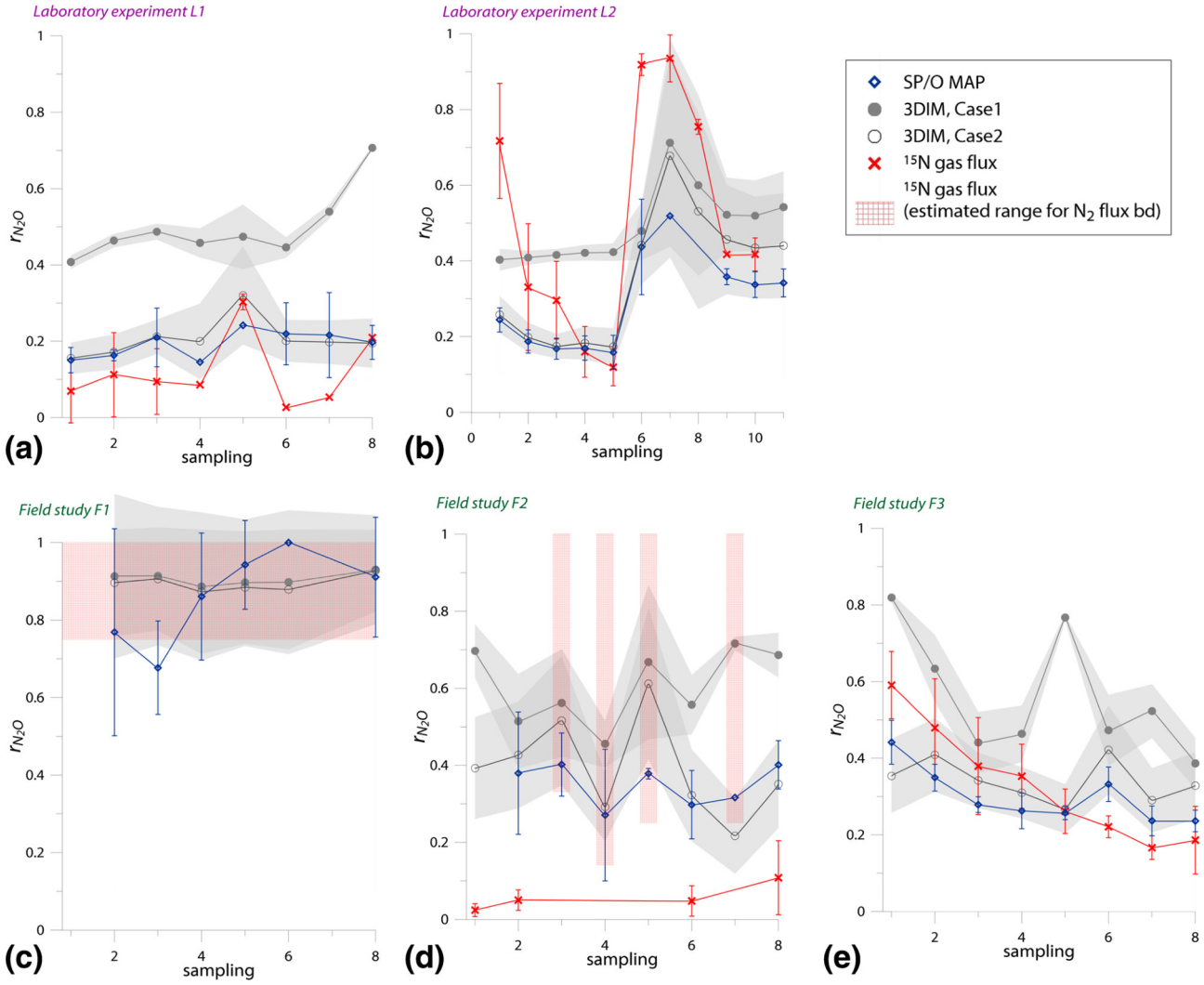

Figure 5. Comparison of time changes in residual N_2O fraction (r_{N_2O}) determined with O/SP MAP Case 1 and 3DIM with the reference method (^{15}N gas flux). For 3DIM results, the 95 % confidence interval is shown with grey shaded areas. Error bars for O/SP MAP and ^{15}N gas-flux data represent the standard deviation of replicate samples ($n = 4$). For N_2 fluxes below the detection limit, the estimated r_{N_2O} values are shown (red areas), calculated with N_2 flux from 0 to 1 of the detection limit.

derived from NH_4^+ pool, but due to rapid NH_4^+ turnover into NO_3^-, we deal with a highly ^{15}N-labeled NO_3^- pool in the $^{15}NH_4^+$ treatment and hence are not able to precisely separate these pools (results not shown).

– With SP/O MAP, we determine the f_{bD} fraction. But since in the SP/O MAP bD and nD cannot be distinguished due to overlapping isotopic signatures (Fig. 1), this fraction actually informs about the bD + nD fraction.

– With 3DIM, we are able to theoretically determine most of the fractions contributing to the N_2O flux, but the precision of such a determination depends on the isotopic separation of particular pathways in the 3D isotopocule plot. In our case study this separation is not very good, especially for $\delta^{15}N$ (see Sect. 3.4); hence, this determination is associated with pronounced uncertainty (Fig. S4).

To compare all these results, we present a comparison of $f_{P\_N_2O}$ of the ^{15}N gas-flux method (representing bD + fD) with f_{bD} of SP/O MAP (representing bD + nD) and respective results (f_{bD}, f_{bD+fD}, f_{bD+nD}) of 3DIM (Fig. 7, Table 4).

A reasonable agreement in the ranges of values is obtained for experiments L1, L2, and F3, but a large disagreement with the reference ^{15}N gas-flux method is observed for field studies F1 and F2 (Table 4). For these studies, extremely low $f_{P\_N_2O}$ was found by the ^{15}N gas-flux method of 0.28 and 0.23, respectively. The time dynamics are not very well reflected by various approaches (Fig. 7). This is mostly visible in F3 (Fig. 7e) where the f_{bD} and f_{bD+fD} show large

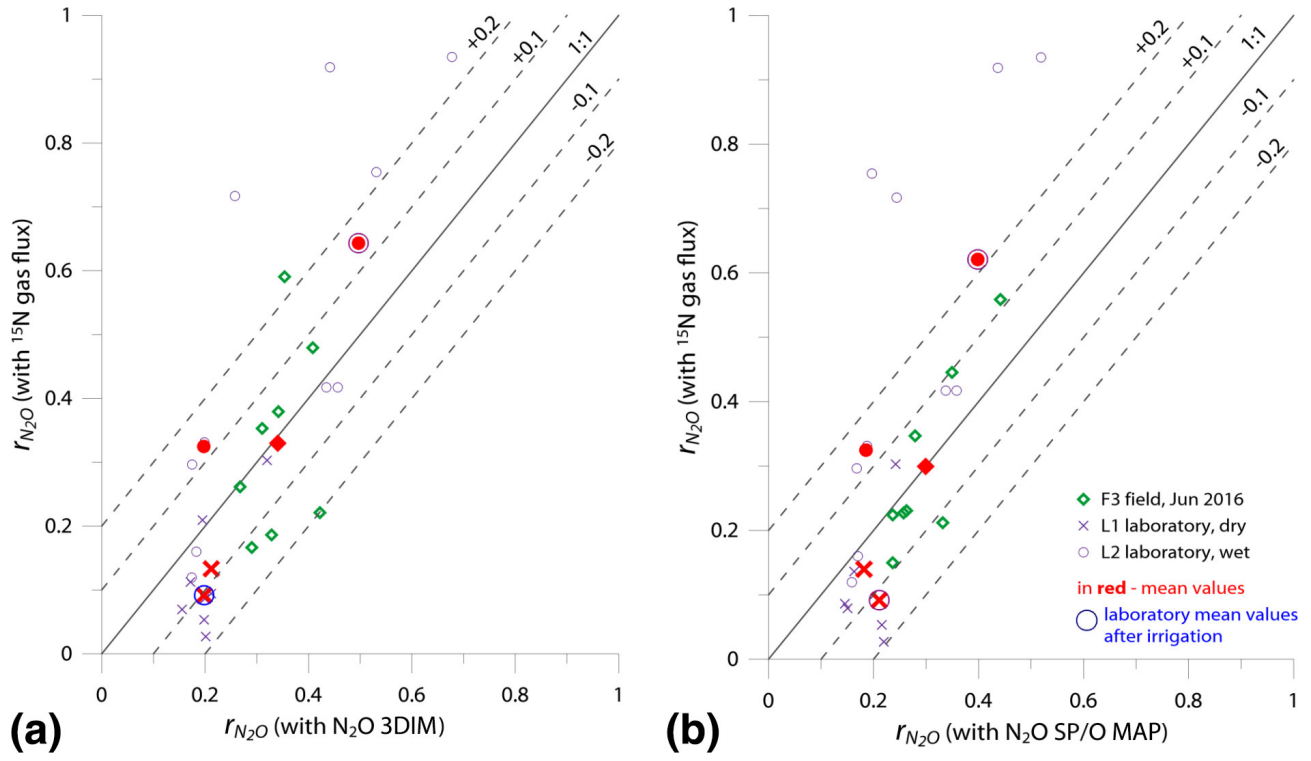

Figure 6. Comparison of 1 : 1 fit between r_{N_2O} determined with the reference method (^{15}N gas flux) and **(a)** 3DIM Case 2 and **(b)** SP/O MAP Case 1.

variations between samplings from below 0.1 to above 0.9. These rapid changes show much lower amplitudes according to the ^{15}N gas-flux approach. The contribution of f_{bD+nD} determined by 3DIM as well as f_{bD} determined by the SP/O MAP is much more stable in time, which is especially clear for F3 (Fig. 7e) but also true for other campaigns (Fig. 7).

For the mixing proportions, the statistical agreement with F value (Eq. 19) cannot be determined, because the fractions provided by various approaches do not precisely refer to the identical pathway contributions and are not directly comparable.

4 Discussion

4.1 MAPs for N_2O data interpretation – opportunities and limitations

So far the interpretations of N_2O isotope data are most commonly done with dual-isotope plots. Whereas SP/N and O/N plots were applied in numerous studies before (Kato et al., 2013; Koba et al., 2009; Opdyke et al., 2009; Ostrom et al., 2007, 2010; Toyoda et al., 2011; Well et al., 2012; Yamagishi et al., 2007; Zou et al., 2014), the usage of the SP/O plot is quite a new idea (Lewicka-Szczebak et al., 2017), but it was already used for field studies (Buchen et al., 2018; Ibraim et al., 2019; Verhoeven et al., 2019). The recent work based on archival datasets with independent estimates of N_2 flux showed some weak accordance of the results of the SP/O MAP with independent estimates (Wu et al., 2019). However, the reasons are difficult to identify for archival data. Here we present the performance of mapping approaches validated with independent estimates based on the ^{15}N gas-flux method, and we try to identify potential problems.

The first challenge, especially for field studies, is obtaining complete datasets. This is due to limited sensitivity of the isotopic measurements and a need for sufficient N_2O and N_2 flux. For our first field study (F1), N_2 flux was under the detection limit and the r_{N_2O} values can thus not be fully compared. For the F2 field study, we have numerous missing data due to N_2O or N_2 flux under the detection limit; hence, only a limited number of data can be compared. This may be the main reason (besides others discussed later – Sect. 4.4) for the weakest accordance of the results for F2. For this field study, only four samples showed the N_2 flux above the detection limit, and these measured N_2 fluxes associated with the low N_2O fluxes yield very low r_{N_2O} values. For samples with N_2 flux below the detection limit, the estimated r_{N_2O} ranges also possibly show much higher values (Fig. 5d). Hence, possibly by missing the measurements of low N_2 fluxes, we miss the higher r_{N_2O} values and our calculated means are not representative of the whole experiment (Table 3).

Table 3. Comparison of N_2O residual fraction (r_{N_2O}) determined with the N_2O isotopocule approaches (SP/O MAP and 3DIM) and the reference method (^{15}N gas flux). Minimal (min), maximal (max), and mean values were calculated with the each sampling mean values (of all replicates). The agreement with the reference method was assessed with the Nash–Sutcliffe efficiency (F, Eq. 19) (Nash and Sutcliffe, 1970), which represents the R^2 of the fit to the 1 : 1 line (Fig. 6).

		N_2O isotopocule approaches				Reference method
		SP/O MAP		3DIM		^{15}N gas flux
		Case 1	Case 2	Case 1	Case 2	
L1	Min	0.15	0.14	0.41	0.16	0.03
	Max	0.24	0.24	0.71	0.32	0.30
	Mean	**0.19**	**0.18**	**0.49**	**0.21**	**0.12**
L2	Min	0.16	0.15	0.40	0.17	0.12
	Max	0.52	0.53	0.71	0.68	0.93
	Mean	**0.27**	**0.27**	**0.49**	**0.36**	**0.50**
F1	Min	0.68	0.70	0.89	0.87	0.75[a]
	Max	1.00	1.00	0.93	0.93	1[a]
	Mean	**0.86**	**0.86**	**0.91**	**0.89**	**nd**[a]
F2	Min	0.30	0.36	0.46	0.22	0.02[b]
	Max	0.43	0.49	0.72	0.61	0.11[b]
	Mean	**0.38**	**0.42**	**0.58**	**0.39**	**0.06**[b]
F3	Min	0.26	0.27	0.39	0.27	0.17
	Max	0.47	0.47	0.82	0.42	0.59
	Mean	**0.33**	**0.32**	**0.54**	**0.34**	**0.33**
Agreement with reference method (***F***)		**0.59*** $p = 0.091$	**0.61*** $p = 0.081$	**−0.09**	**0.77**** $p = 0.015$	

[a] all N_2 fluxes under detection limit, the range of values estimated based on detection limit – values not included in the statistics
[b] data not complete due to half of N_2 fluxes under detection limit – values not included in the statistics

SP/O MAP

The SP/O MAP was proposed (Lewicka-Szczebak et al., 2017) after it was found that $\delta^{18}O$ of the N_2O produced by bacterial and fungal denitrification is quite stable and together with SP may be useable for discrimination of these pathways (Lewicka-Szczebak et al., 2016; Rohe et al., 2014a). As O precursor for bD, fD, and nD the soil water is accepted, under the assumption of nearly complete O exchange between water and denitrification intermediates. The high extent of O exchange during denitrification has been confirmed experimentally (Kool et al., 2009; Lewicka-Szczebak et al., 2016; Rohe et al., 2014b), and it results in a quite stable range for mixing endmember values for $\delta^{18}O$ for bacterial and fungal denitrification (Fig. 1). Importantly, due to a higher isotope fractionation effect associated with subsequent reduction steps of NO_3^- to N_2O (i.e., removal of oxygen atoms, so called branching effect) during fungal denitrification, the ranges for $\delta^{18}O$ of bacterial and fungal N_2O differ significantly (Lewicka-Szczebak et al., 2016). Fungal denitrification shows very consequent high O exchange and high fractionation during O branching (Rohe et al., 2014b, 2017), whereas bacterial denitrification is characterized, in general, by lower fractionation, but the differences in both fractionation and O exchange between particular bacterial strains are large (Rohe et al., 2017). As a result of lower O exchange shown by some bacterial strains, $\delta^{18}O_{NO_3^-}$ is also incorporated into produced N_2O (Rohe et al., 2017). This complicates the application of the proposed SP/O MAP. It is not clear how large the importance of such bacterial strains is in soil communities. We assume it must be low, because soil incubation studies indicated so far mostly very high exchange rates (Kool et al., 2007; Kool et al., 2009; Lewicka-Szczebak et al., 2016). These studies covered in total 16 soils. Only for two forest soils characterized by very low N_2O emission was the O exchange around 20 % (Kool et al., 2009) and otherwise over 60 %, with mean of around 90 % (Kool et al., 2009; Lewicka-Szczebak et al., 2016). Importantly, the range of $\delta^{18}O$ values determined for bacterial denitrification does not assume complete O exchange but is determined for the soil samples of O exchange varying in the range from 63 % to 100 % (Lewicka-Szczebak et al., 2016). Hence, based on current knowledge, this can be assumed typical for most soils and experimental conditions. Also in this study, quite a good agreement of the r_{N_2O} determined by the O/SP MAP and the reference method (see Sect. 3.6) allows us to confirm the general assumption underlying this calculation method.

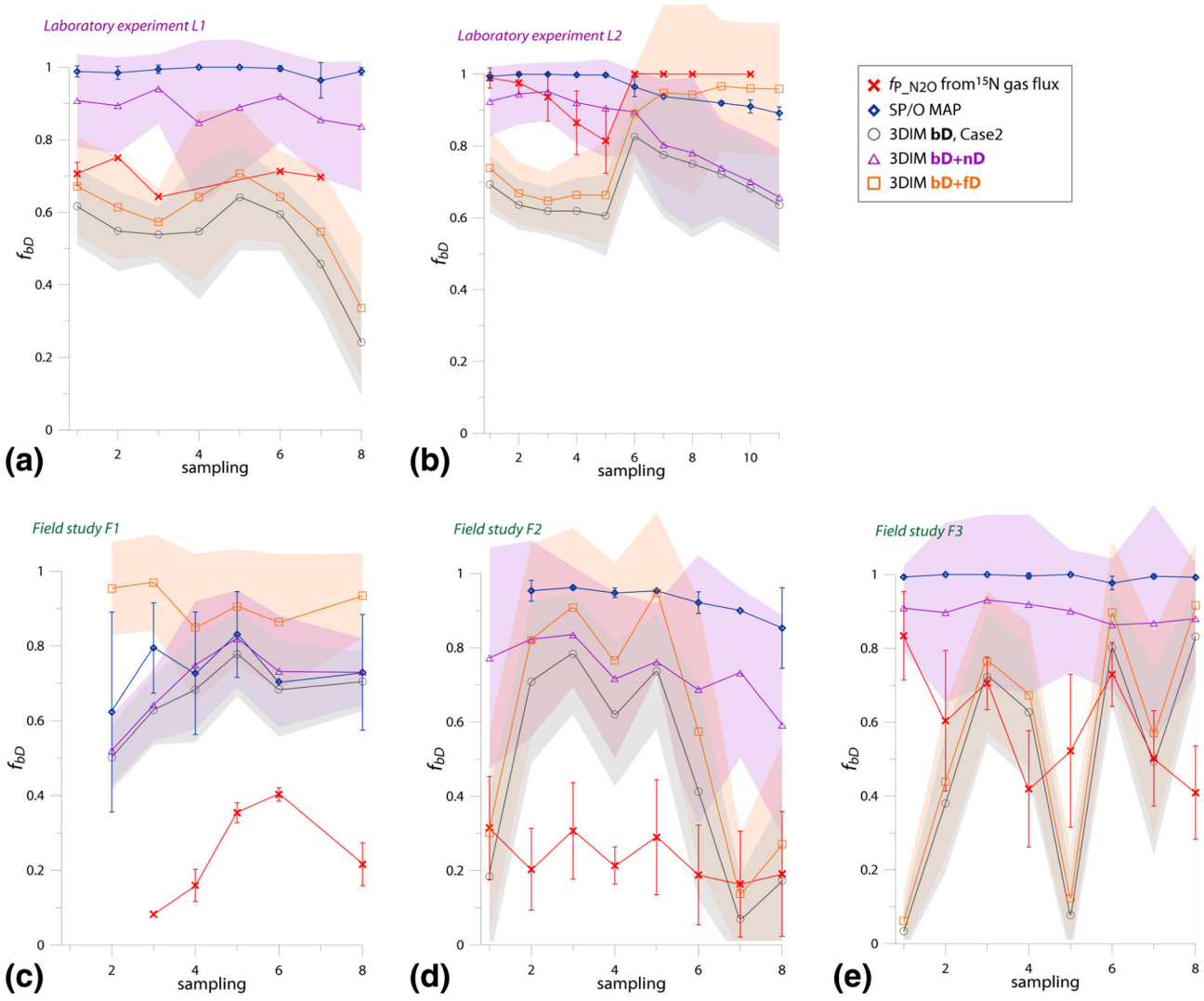

Figure 7. Comparison of N_2O fractions comprising bacterial denitrification (f_{bD}) determined with O/SP MAP Case 1 (representing bD + nD) and 3DIM Case 2 (respective fractions determined: bD, bD + nD, bD + fD) with the reference method (^{15}N gas flux). The ^{15}N gas-flux method determines the $f_{P\_N_2O}$ – ^{15}N-pool-derived fraction – comprising all N_2O origins utilizing ^{15}N-labeled NO_3^- – theoretically mostly bD and fD. See Sect. 4.2 and 4.3 for further discussion. For 3DIM results, the 95 % confidence interval is shown with shaded areas. Error bars for O/SP MAP and ^{15}N gas-flux data represent the standard deviation of replicate samples ($n = 4$).

SP/N MAP

The application of dual-isotope plot SP/N was initially proposed by Yamagishi et al. (2007) for ocean waters and by Koba et al. (2009) for groundwater studies. In open water bodies, the application of SP/N MAP might be effective due to relatively homogenous distribution of substrates in the sampled water volume and thus not biased by the spatial heterogeneity in ^{15}N enrichment that can occur in soils due to the fractionation processes in soil microsites (Bergstermann et al., 2011; Cardenas et al., 2017; Castellano-Hinojosa et al., 2019; Lewicka-Szczebak et al., 2015; Well et al., 2012). The $\delta^{15}N$ isotopic signatures of samples were corrected for NO_3^- substrate only, and for water studies this approach was well justified by the complete conversion of NH_4^+ to NO_3^- (Koba et al., 2009). This assumption was based on the low NH_4^+ concentration and should result in equal $\delta^{15}N$ of NH_4^+ and NO_3^-, which justified putting the whole dataset into a single $\delta^{15}N^{SP} - \delta^{15}N$ scheme. But for soil studies, due to multiple possible N substrates and difficulties to find a proper correcting strategy, later studies rather applied bulk measured $\delta^{15}N$ without corrections (Kato et al., 2013; Toyoda et al., 2011). Up to now, the most appropriate approach of taking precursors into account is the recalculation of literature mixing endmember values to the actually measured substrate values for each particular pathway, namely, NO_3^- for denitrification and NH_4^+ for nitrification (Zou et al., 2014). But this approach was not successful for this study (see Sect. 3.4).

Table 4. Comparison of N_2O fraction originating from bD (f_{bD}) determined with the N_2O isotopocule approaches (SP/O MAP and 3DIM) and the reference method (^{15}N gas flux). Due to methodical assumptions for the particular approach, either the bD + nD fraction (for SP/O map and 3DIM) or the bD + fD fraction (for 3DIM and the reference method) can be compared (see Sect. 3.7).

		N_2O isotopocule approaches						Reference method
		SP/O MAP (bD + nD)		3DIM (bD + nD)		3DIM (bD + fD)		^{15}N gas flux (bD + fD)
		Case 1	Case 2	Case 1	Case 2	Case 1	Case 2	
L1	Min	0.96	0.79	0.86	0.84	0.35	0.34	0.64
	Max	1	1	0.94	0.94	0.71	0.71	0.75
	Mean	**0.99**	**0.93**	**0.89**	**0.89**	**0.59**	**0.59**	**0.70**
L2	Min	0.94	0.88	0.65	0.66	0.65	0.65	0.81
	Max	1	1	0.95	0.95	0.97	0.97	1
	Mean	**0.98**	**0.96**	**0.84**	**0.84**	**0.82**	**0.82**	**0.95**
F1	Min	0.62	0.55	0.52	0.52	0.85	0.85	0.08
	Max	0.84	0.83	0.82	0.82	0.97	0.97	0.42
	Mean	**0.74**	**0.70**	**0.70**	**0.70**	**0.91**	**0.91**	**0.28**
F2	Min	0.84	0.64	0.62	0.59	0.34	0.14	0.16
	Max	0.95	0.89	0.83	0.83	0.94	0.95	0.31
	Mean	**0.92**	**0.77**	**0.75**	**0.74**	**0.65**	**0.59**	**0.23**
F3	Min	0.97	0.92	0.87	0.86	0.21	0.06	0.41
	Max	1	1	0.93	0.93	0.92	0.92	0.83
	Mean	**0.99**	**0.97**	**0.90**	**0.90**	**0.60**	**0.56**	**0.59**

When endmember mixing areas were recalculated with the measured substrate isotope signatures, most of the sampling points were located outside the mixing-reduction area. This is most probably due to large variations in isotopic signatures of the substrates and the fact that the analyzed bulk $\delta^{15}N$ values are not representative of the actually utilized substrate pools due to spatial heterogeneity of fractionating processes as outlined above. Moreover, the range of values for NH_4^+ and NO_3^- of our studies resulted in a very untypical location of endmember ranges for denitrification and nitrification MAPs (Figs. 2 and 3); hence, the method is not really suitable for discriminating mixing of these pathways and N_2O reduction for this particular study. This is due to the extremely high $\delta^{15}N_{NH_4}$ values (even up to 100 ‰), which are associated with low NH_4^+ contents (Table 2). This indicates that the ammonium pool was highly fractionated and nearly exhausted. This fast ammonium consumption will be further investigated in a follow-up paper by applying the Ntrace model, where we also apply the $^{15}NH_4$ treatment for its proper interpretation (Müller et al., 2014).

O/N MAP

After it was observed that N_2O reduction results in the typical O/N slope of 2.6 (Menyailo and Hungate, 2006; Ostrom et al., 2007; Well and Flessa, 2009), the O/N MAP was proposed for identification of significant N_2O reduction based on the observed slope higher than 1 (Opdyke et al., 2009; Ostrom et al., 2007). However, it must be noted that in the case of temporal shifts in the isotopic composition of the N or O substrate, the assessment of the importance of N_2O reduction is not valid (Ostrom et al., 2010). This approach was well suited for short-term controlled experiments; however, for longer field studies, where we deal with large variations of N substrate isotopic signatures, application of this approach appears problematic. We plotted our data in the O/N MAP and found a significant linear relationship for field and laboratory studies, both with very similar equations. The observed slopes of 0.24 and 0.28, respectively, are much below 1, although the N_2O reduction shows important contribution for these experiments (Table 3). Hence, this observed slope is rather due to change of active substrate pool or changes in the isotopic fractionation (Cardenas et al., 2017). This might be a result of changes in soil moisture during experiments (irrigation or rain episodes). The observed shift in $\delta^{15}N$ is ca. 4 times larger than for $\delta^{18}O$. We suppose that water addition intensified N_2O production, and this might have caused significant enrichment in active nitrate pool in soil microsites. For O isotopes, intensified N_2O production may result in slightly lower O exchange, which may increase the $\delta^{18}O$ values as a result of incorporation of nitrate O signature (Lewicka-Szczebak et al., 2015; Rohe et al., 2017). Consequently, the isotope effects due to reduction are significantly interfered by shifts in N_2O precursor dynamics. Since for this MAP both N and O isotopes depend on the precursor isotopic signature and are significantly altered by the diffusion (Well and Flessa, 2008), the interpretations based on this MAP are the most ambiguous.

4.2 3DIM – perspectives of this new approach

Such a model for interpretation of N_2O isotopic data is proposed here for the first time. This model is based on the Bayesian mixing models, being a well-established and widely applied method in food-web studies to partition dietary proportions (Parnell et al., 2013; Phillips et al., 2014). But for N_2O the determination of mixing proportion of different pathways contributing to N_2O production is further complicated by N_2O reduction, which alters the final N_2O isotopic signature. This additional parameter was incorporated into the model equations (Eqs. 13, 14). Moreover, it is still not clarified if the reduction of N_2O produced during bacterial denitrification only is possible (Case 1) or also N_2O from other pathways can be further reduced by bacterial denitrifiers (Case 2); hence, both cases need to be considered. The model has a few advantages over the SP/O MAP. First of all, it allows for including uncertainties in input data into the model and allows for assessment of the confidence intervals for the results. Moreover, theoretically 3DIM allows for separation of four N_2O production pathways, currently identified as the most relevant, within them f_{fD}, which is so far not distinguishable with other isotopic methods (Wrage-Mönnig et al., 2018).

For our case studies, it has been shown that $\delta^{15}N$ values are not useful in dual-isotope plots for quantitative estimations (Figs. 2 and 3, Sect. 3.4) but are helpful to constrain mixing proportions when incorporated into 3DIM. Since the model is based on a probability distribution, it allows for providing estimates even for imprecise data, e.g., as in our case by difficulties in proper determination of $\delta^{15}N$ endmember ranges due to very unstable precursor isotopic signatures.

The model outputs allow us to assess the quality of model performance and reliability of the results (Fig. S4, Sect. 3.5). From the uncertainty analysis provided by the model, we can determine the confidence intervals for the estimated values (Figs. 5 and 7). This is a total uncertainty resulting from all possible uncertainty sources due to ranges of endmember values and fractionation factors, variations in N_2O isotopic signatures for one sampling date, and convergence of possible model results for three isotopic signatures. We are not able to separate these uncertainties in this study.

Another measure of model performance is given by the correlations between obtained results of all the modeled probable solutions (Fig. S4). Previous studies applying similar models interpreted the strong negative correlations between determined mixing proportions as inability of the model to distinguish these sources (Moore and Semmens, 2008; Parnell et al., 2013; Phillips et al., 2014). We observe strong negative correlations between f_{bD} and f_{nD} for most cases. This may indicate the uncertainty in determination of these fractions due to the lack of isotopic separation of these processes in the $\delta^{15}N^{sp}/\delta^{18}O$ space (Fig. 1). But such a correlation is also expected if we deal with two strongly dominating sources, and the correlations between f_{bD} and f_{nD} are indeed highest for F3, where the fractions of other pathways are lowest. Nevertheless, for fractions showing high correlations, presentation of the sum of these pathways may be much more informative than separation between them. Therefore, we observe much more stable results for the sum of f_{bD} and f_{nD} than for f_{bD} alone (Fig. 7). However, the large variations of f_{bD} are not only the modeling artifact but they also reflect the variations noted with the reference method, which is especially clear for F3 (see Fig. 7e). In this case study, we can see that the variations of f_{bD} are larger than in the reference method, but similar dynamics of these variations can be observed.

With the model, we can quantify the contribution of four pathways; however, there are so far no precise enough reference methods to validate these results (Wrage-Mönnig et al., 2018) (see Sect. 3.7). But are the provided estimates plausible? We can check with the most characteristic outcomes. For F1, the highest f_{fD} values were noted (Fig. 4). For this field study, also the highest r_{N_2O} and the lowest f_{bD} were noted by all the approaches (Tables 3 and 4, Figs. 5c and 7c). Since for fD N_2O is mostly the final product not further reduced to N_2 (Sutka et al., 2008), the higher f_{fD} should result in higher r_{N_2O} values, which was noted for F1. The highest f_{Ni} was noted for F2. In this field study, the soil ammonium content is clearly the highest and nitrate the lowest (Table 2), which indicates that nitrification can be more active here during the whole study campaign, when compared to the other experiments, where we deal with large ammonium consumption at the very beginning of the experiments. This accordance of results allows us to suppose that the general trends in pathway mixing proportions provided by the model is plausible.

4.3 Agreement in estimates of isotopocule approaches and independent estimates

In general, the both cases of SP/O MAP and Case 2 of 3DIM show very similar results, whereas Case 1 of 3DIM indicates always higher r_{N_2O} values and hence underestimates N_2 flux (Table 3, Fig. 5). For the SP/O MAP, the application of different calculation cases has little impact on the final results because both cases show very high and quite stable f_{bD}. The contribution of bD is expressed jointly with nD for the SP/O MAP, due to their isotopic overlap (see Sect. 3.4). As a result, the necessary assumption for the SP/O MAP is the possible reduction of N_2O originating from both of these fractions (bD and nD, also for Case 1). Conversely for 3DIM, both these fractions are separated, and for Case 1 only the bD fraction can be reduced. The r_{bD} values obtained for Case 1 are very low (e.g., 0.2 for F2 and 0.15 for F3), but when recalculated to r_{N_2O} (for comparison with other results), they become high (e.g., 0.58 for F2 and 0.54 for F3, Table 3) due to respective f_{bD} values (see Eq. 15). Therefore, the r_{N_2O} determined by 3DIM Case 1 is very vulnerable to proper determination of f_{bD}. And this fraction is not very precisely determined, as we know from strong correlation found for

f_{bD}/f_{nD} (see Sect. 4.2). Consequently, the imprecise separation of f_{bD} and f_{nD} is the reason for the biased r_{N_2O} values for Case 1 3DIM. This bias is not significant when we deal with very high r_{N_2O} fraction, as for F1 (Table 3) or for very high and stable bD contribution, as for L2 (Table 3, Fig. 7b). For Case 2, the lack of precision in f_{bD} and f_{nD} determination do not largely affect r_{N_2O} results, since N_2O originating from all pathways can be reduced in this case (Eq. 14). Hence, in further discussion of the 3DIM results, we take into account Case 2 outputs only. This observation may also indicate that it is not just N_2O from heterotrophic bacterial denitrification that can be further reduced to N_2. Although previous studies suggested Case 1 to be more accurate (Verhoeven et al., 2019; Wu et al., 2019), our comparison indicates that Case 1 of 3DIM underestimates the N_2O reduction in most cases (Table 3). This may reinforce a recent discussion on nitrifier denitrification mechanisms assuming that heterotrophic bacterial denitrifiers are relevant in reducing NO_2^- from nitrification (Hink et al., 2017). This would support the assumption that N_2O from nD can be further reduced by the bD pathway.

The largest discrepancy in r_{N_2O} between isotopocule approaches and the reference method is noted for F2 (Table 3). In this field campaign we deal with very low N_2O fluxes and the reference method indicates very low r_{N_2O} values, i.e., very high N_2O reduction rate. Moreover, for F2 the highest soil moisture of the field studies was noted (Table 2), which may result in inhibition of gaseous exchange. In these conditions, it is very probable that some of the produced N_2O is completely reduced; consequently, the isotopic information on its reduction is missed. Complete N_2O reduction in soil microsites would result in overestimation of r_{N_2O} values by the N_2O isotopocule approaches, and this is what we observe in this case (Fig. 5d).

Pronounced discrepancies in mean values are also noted for L2 laboratory incubation (Table 3), which is due to rapid changes in r_{N_2O} resulting from water addition (Fig. 5b, Sect. 4.1). This rapid change is noted in both SP/O MAP and 3DIM as well as in the reference method, but the N_2O isotopocule results seem to react slower and with lower amplitude. N_2O isotopocule approaches are based on isotopic analyses of N_2O, whereas the ^{15}N gas-flux method is based on the direct N_2 measurements. If N_2O is partially stored in soil we may deal with a delay in our observations or discrepancy in results. This indicates that individual sudden changes are not well monitored by the isotopocule approaches, but the general mean values and changing trends are very well reflected (Table 3, Fig. 6).

Summary statistics for agreement between isotopocule approaches and the reference method indicate significant fit for SP/O MAP, where both cases show very similar fit, and for 3DIM Case 2, where the best fit was observed (Table 3). This agreement is much better than recently shown by Wu et al. (2019), where numerous cases with very poor agreement between the results of O/SP MAP and the reference method have been found. That study analyzed archival datasets, from which many experiments consisted of various experimental phases – like anoxic and oxic or before and after fertilizer addition. This might have complicated the comparability of the results. As shown by our study, the sudden changes in experimental conditions are differently reflected in the results of both methods. Whereas the reference method based on direct measurements of N_2 flux reacts immediately, results of isotopocule approaches show a certain delay, possibly due to accumulation of N_2O in the soil (Fig. 5b). But when we compare the mean values for each experimental phase, the agreement between both methods is much better (Fig. 6). Additionally, the former study included some experiments with glucose amendment (Wu et al., 2019), which results in a very rapid N turnover and consequently unstable pathway contribution.

The source partitioning of N_2O production seems much more problematic than of r_{N_2O} values. This is also more difficult to be evaluated with the reference method since it yields only the sum of fD and bD, i.e., it does not distinguish these individual processes (see Sect. 3.7). We are also aware that the model may not be very precise in separation of f_{bD}, f_{nD}, and f_{fD}, since they often show strong negative correlations (see Sects. 3.5 and 4.2). Taking these considerations into account, we can understand the fraction contributions for L1, L2, and F3, where the f_{bD} fraction of SP/O MAP and f_{bD+nD} of 3DIM are comparable, and f_{bD+fD} of 3DIM and $f_{P\_N_2O}$ of the ^{15}N gas-flux method show similar range and trends (Fig. 7a, b, and e). However, a large bias in source partition is observed for F1 and F2 field studies. The $f_{P\_N_2O}$ determined by the ^{15}N gas-flux method is much lower than any fraction determined with isotopocule methods (Fig. 7c and d). The very low $f_{P\_N_2O}$ fraction indicates a large contribution of N_2O originating from the unlabeled pool, since the $f_{P\_N_2O}$ of the labeled $^{15}NH_4^+$ treatment was also comparably low (data not shown). This N_2O may originate from the organic N pool pathway (Müller et al., 2014; Zhang et al., 2015) or chemodenitrification (Wei et al., 2019). These processes are not included in the isotopocule methods and hence cannot be accounted for. For these two field studies (F1 and F2), we deal with relatively low fluxes and low temperatures; thus, the processes invisible for high flux situations may play a significant role here.

4.4 Possible origins of inconsistency and potential improvements

From the comparison of isotopocule approaches and the reference method, we can identify the condition when the calculation based on natural abundance N_2O isotopes may be biased. The MAPs applying $\delta^{15}N$ values are very vulnerable to changes in substrate isotopic signatures. When we observe large variations in soil NO_3^-, NO_2^-, or NH_4^+ isotopic signatures, such an approach should rather not be applied.

Most problematic is the occurrence of N_2O production pathways which are so far not investigated for their charac-

teristic isotopic signature. This might be heterotrophic nitrification, co-denitrification, or chemodenitrification, as supposed for our case studies F1 and F2. These less examined processes gain in significance when the N_2O fluxes are generally low, like in F1 and F2, where N_2O flux was mostly below 10 g N-N_2O ha^{-1} d^{-1}. Hence, for such low N_2O fluxes application of isotope MAPs and 3DIM may be less precise.

Recent literature suggest that the most vulnerable value for SP/O MAP is the isotopic signature of the bD mixing endmember, and this parameter should be best determined in focused experiments (Buchen et al., 2018; Wu et al., 2019). It was shown that a short-term anoxic experiment with N_2O reduction inhibition with C_2H_2 favors bD (Lewicka-Szczebak et al., 2017; Lewicka-Szczebak et al., 2016). Such an experiment could have been used for determination of isotopic signature of bacterial denitrification characteristic for the particular soil used in this study and narrow the range of mixing endmember for bD pathway. Unfortunately, when planning and conducting these studies, we did not have this complete knowledge and missed the opportunity to perform such parallel anoxic incubations, but this should be strongly recommended for further studies applying SP/O MAP or 3DIM.

The determination of initial delta values (δ_0), unchanged by N_2O reduction, might also be helpful in further constraining the isotope MAPs. These δ_0 can be obtained from the relation of r_{N_2O} determined by reference method and measured isotopic signatures (Lewicka-Szczebak et al., 2017). Unfortunately, this approach was not successful for our data, because no significant correlation between r_{N_2O} and isotopic signatures could be found. This indicates unstable endmember mixing proportions or some problems with parallel experiments. This was also the case in previous validation experimental study (Lewicka-Szczebak et al., 2017), where for oxic conditions the variations were too high to obtain significant correlation and determine the δ_0 values. This shows that oxic experiments are not well suited for determination of isotopic signatures of particular mixing endmembers and should be always accompanied by more focused and stable anoxic incubations.

Further enhancement in performance of the isotope MAPs could be attained if the experiments determining the initial isotopic composition of mixing endmembers were performed with the soil collected parallel to particular experiments, and the anoxic incubations were performed in conditions similar to field conditions during the particular case study. Possibly from such experiments, some subtle differences in characteristic endmember isotopic signatures could be detected. It can be supposed that such differences could be the reason for worse r_{N_2O} agreement with reference method for L2 and F2 (Table 3). It has been shown that the changes in initial $\delta^{18}O$ value of bacterial denitrification endmember has a significant impact on the final results (Wu et al., 2019). We have checked if this could bring better agreement. For L2, a perfect agreement of SP/O MAP and the reference method is obtained when applying slightly higher $\delta^{18}O$ values (25 ‰ instead of 19 ‰). Conversely for F2, much lower $\delta^{18}O$ values (10 ‰ instead of 19 ‰) would be needed to obtain the perfect agreement. These differences are quite possible: the low values for F2 might be a result of low temperature and low fluxes and consequently moderate or slow processes associated with maximal O exchange. On the contrary, for high water content and high temperature in the L2 experiment, we can expect slightly lower O exchange, resulting in higher initial $\delta^{18}O$ values.

5 Conclusions

- It was shown that the N_2O residual fraction can be calculated based on isotope fractionation during N_2O reduction with SP/O MAP. The SP/N MAP appeared more complex and problematic.

- Here we present for the first time the idea of applying a model based on three N_2O isotopic signatures. We are convinced that this is a powerful step forward in the development of N_2O isotopocule methods to especially quantify r_{N_2O} but also to estimate some mixing proportions of the four N_2O pathways included in the model.

- Both N_2O isotopocule-based approaches – SP/O MAP and 3DIM (Case 2) – show good accordance of r_{N_2O} with reference method and very comparable results to each other. For 3DIM, the results of Case 1 (assuming N_2O reduction of bacterial denitrification only) underestimate the N_2 flux due to imprecision in determination of f_{bD}.

- The determination of mixing proportions with N_2O isotopocule-based approaches is biased for cases where additional processes not incorporated into the model occur. This may be the case when very low N_2O fluxes are noted.

- N_2 flux determined from ^{15}N-labeled treatments (reference method) show more rapid changes compared to values determined with N_2O isotopocule approaches. Hence, the r_{N_2O} determined with N_2O isotopocule approaches provides a good approximation of the averaged N_2O reduction range, but does not reflect dynamic changes in r_{N_2O} with high resolution.

- 3DIM allows for a good control of the results quality, which is a clear advantage over the results provided with SP/O MAP.

- According to these findings, the SP/O MAP and 3DIM can be applied for r_{N_2O} determination with an expected precision of around 0.15. For cases where the mixing proportion separation is imprecise, which can be supposed when model results show high negative correlations, the results should be carefully interpreted, and

preferably the values of correlated fractions should be shown jointly. In such cases, the calculation for Case 2 should be applied for r_{N_2O} determination, since Case 1 incorporates possibly biased f_{bD} values into the final r_{N_2O} value. Importantly, even for these cases where the determination of mixing proportions was biased, we got reasonable estimates of r_{N_2O} values (with Case 2 calculations).

Data availability. Original data are available upon request. Material necessary for this study's findings is presented in the paper and the Supplement.

Supplement. The supplement related to this article is available online at: https://doi.org/10.5194/bg-17-5513-2020-supplement.

Author contributions. DLS and RW designed the field studies and laboratory experiments, and DLS was in charge of caring them out. DLS performed the interpretations based on isotope mapping approaches and initiated the idea of the three-dimensional model. MPL developed the model and provided results for analyzed case studies with graphical presentations. DLS prepared the article with significant contributions from RW and MPL.

Competing interests. The authors declare that they have no conflict of interest.

Acknowledgements. Many thanks are due to Frank Hegewald and Nicolas Ruoss for help in conducting field studies, Stefan Burkart for help in carrying out soil incubation, Martina Heuer for help in isotopic analyses, Nicole Altwein and Ute Tambor for help in preparing laboratory incubation and in soil analyses Kerstin Gilke for chromatographic analyses and Caroline Buchen for advice in preparing field campaigns.

Financial support. This research has been supported by the German Research Foundation (DFG, grant nos. LE 3367/1-1 and WE 1904/10-1). This Open Access Publication was financed by the Open Access Grant Program of the German Research Foundation (DFG) (grant nos. LE 3367/1-1) and the Open Access Publication Fund of the University of Göttingen.

Review statement. This paper was edited by Perran Cook and reviewed by two anonymous referees.

References

Aulakh, M. S., Doran, J. W., and Mosier, A. R.: Field-Evaluation of 4 Methods for Measuring Denitrification, Soil Sci. Soc. Am. J., 55, 1332–1338, 1991.

Baily, A., Watson, C. J., Laughlin, R., Matthews, D., McGeough, K., and Jordan, P.: Use of the ^{15}N gas flux method to measure the source and level of N_2O and N_2 emissions from grazed grassland, Nutr. Cycl. Agroecosys., 94, 287–298, 2012.

Barford, C. C., Montoya, J. P., Altabet, M. A., and Mitchell, R.: Steady-state nitrogen isotope effects of N_2 and N_2O production in Paracoccus denitrificans, Appl. Environ. Microb., 65, 989–994, 1999.

Baumgärtel, B. and Benke, M.: Düngeempfehlungen Stickstoff: Getreide, Raps, Hackfrüchte, Landwirtschaftskammer Niedersachsen – Geschäftsbereich Landwirtschaft, Hannover, 2009.

Bergsma, T. T., Ostrom, N. E., Emmons, M., and Robertson, G. P.: Measuring simultaneous fluxes from soil of N_2O and N_2 in the field using the ^{15}N-Gas "nonequilihrium" technique, Environ. Sci. Technol., 35, 4307–4312, 2001.

Bergstermann, A., Cardenas, L., Bol, R., Gilliam, L., Goulding, K., Meijide, A., Scholefield, D., Vallejo, A., and Well, R.: Effect of antecedent soil moisture conditions on emissions and isotopologue distribution of N_2O during denitrification, Soil Biol. Biochem., 43, 240–250, 2011.

Böhlke, J. K., Smith, R. L., and Hannon, J. E.: Isotopic analysis of N and O in nitrite and nitrate by sequential selective bacterial reduction to N_2O, Anal. Chem., 79, 5888–5895, 2007.

Bouwman, A. F., Beusen, A. H. W., Griffioen, J., Van Groenigen, J. W., Hefting, M. M., Oenema, O., Van Puijenbroek, P. J. T. M., Seitzinger, S., Slomp, C. P., and Stehfest, E.: Global trends and uncertainties in terrestrial denitrification and N_2O emissions, Philos. T. R. Soc. B, 368, https://doi.org/10.1098/rstb.2013.0112, 2013.

Brenninkmeijer, C. A. M. and Röckmann, T.: Mass spectrometry of the intramolecular nitrogen isotope distribution of environmental nitrous oxide using fragment-ion analysis, Rapid Commun. Mass Sp., 13, 2028–2033, 1999.

Buchen, C., Lewicka-Szczebak, D., Fuß, R., Helfrich, M., Flessa, H., and Well, R.: Fluxes of N_2 and N_2O and contributing processes in summer after grassland renewal and grassland conversion to maize cropping on a Plaggic Anthrosol and a Histic Gleysol, Soil Biol. Biochem., 101, 6–19, 2016.

Buchen, C., Lewicka-Szczebak, D., Flessa, H., and Well, R.: Estimating N_2O processes during grassland renewal and grassland conversion to maize cropping using N_2O isotopocules, Rapid Commun. Mass Sp., 32 (13), 1053–1067, 2018.

Butterbach-Bahl, K., Baggs, E. M., Dannenmann, M., Kiese, R., and Zechmeister-Boltenstern, S.: Nitrous oxide emissions from soils: how well do we understand the processes and their controls?, Philos. T. R. Soc. B, 368, https://doi.org/10.1098/rstb.2013.0122, 2013.

Cardenas, L. M., Bol, R., Lewicka-Szczebak, D., Gregory, A. S., Matthews, G. P., Whalley, W. R., Misselbrook, T. H., Scholefield, D., and Well, R.: Effect of soil saturation on denitrification in a grassland soil, Biogeosciences, 14, 4691–4710, https://doi.org/10.5194/bg-14-4691-2017, 2017.

Casciotti, K. L., Sigman, D. M., Hastings, M. G., Bohlke, J. K., and Hilkert, A.: Measurement of the oxygen isotopic composition of

nitrate in seawater and freshwater using the denitrifier method, Anal. Chem., 74, 4905–4912, 2002.

Castellano-Hinojosa, A., Loick, N., Dixon, E., Matthews, G. P., Lewicka-Szczebak, D., Well, R., Bol, R., Charteris, A., and Cardenas, L.: Improved isotopic model based on ^{15}N tracing and Rayleigh-type isotope fractionation for simulating differential sources of N_2O emissions in a clay grassland soil, Rapid Commun. Mass Sp., 33, 449–460, 2019.

Decock, C. and Six, J.: An assessment of N-cycling and sources of N_2O during a simulated rain event using natural abundance ^{15}N, Agr. Ecosyst. Environ., 165, 141–150, 2013.

Eschenbach, W., Lewicka-Szczebak, D., Stange, C. F., Dyckmans, J., and Well, R.: Measuring ^{15}N Abundance and Concentration of Aqueous Nitrate, Nitrite, and Ammonium by Membrane Inlet Quadrupole Mass Spectrometry, Anal. Chem., 89, 6076–6081, 2017.

Felix, J. D., Elliott, E. M., Gish, T. J., McConnell, L. L., and Shaw, S. L.: Characterizing the isotopic composition of atmospheric ammonia emission sources using passive samplers and a combined oxidation-bacterial denitrifier approach, Rapid Commun. Mass Sp., 27, 2239–2246, 2013.

Firestone, M. K. and Davidson, E. A.: Microbial basis of NO and N_2O production and consumption in soil, in: Exchange of trace gases between terrestial ecosystems and the atmosphere, edited by: Andreae, M. O. and Schimel, D. S., John Wiley and Sons, New York, 1989.

Frame, C. H. and Casciotti, K. L.: Biogeochemical controls and isotopic signatures of nitrous oxide production by a marine ammonia-oxidizing bacterium, Biogeosciences, 7, 2695–2709, https://doi.org/10.5194/bg-7-2695-2010, 2010.

Fuß, R.: R-Package: Gasfluxes, available at: https://bitbucket.org/ecoRoland/gasfluxes (last access: 10 January 2020), 2015.

Groffman, P. M.: Terrestial denitrification: challenges and opportunities, Ecol. Process., 1, 1–11, 2012.

Groffman, P. M., Altabet, M. A., Bohlke, J. K., Butterbach-Bahl, K., David, M. B., Firestone, M. K., Giblin, A. E., Kana, T. M., Nielsen, L. P., and Voytek, M. A.: Methods for measuring denitrification: Diverse approaches to a difficult problem, Ecol. Appl., 16, 2091–2122, 2006.

Hink, L., Lycus, P., Gubry-Rangin, C., Frostegård, A., Nicol, G. W., Prosser, J. I., and Bakken, L. R.: Kinetics of NH_3^- oxidation, NO^- turnover, N_2O^- production and electron flow during oxygen depletion in model bacterial and archaeal ammonia oxidisers, Environ. Microbiol., 19, 4882–4896, 2017.

Hutchinson, G. L. and Mosier, A. R.: Improved Soil Cover Method for Field Measurement of Nitrous Oxide Fluxes, Soil Sci. Soc. Am. J., 45, 311–316, 1981.

Ibraim, E., Wolf, B., Harris, E., Gasche, R., Wei, J., Yu, L., Kiese, R., Eggleston, S., Butterbach-Bahl, K., Zeeman, M., Tuzson, B., Emmenegger, L., Six, J., Henne, S., and Mohn, J.: Attribution of N_2O sources in a grassland soil with laser spectroscopy based isotopocule analysis, Biogeosciences, 16, 3247–3266, https://doi.org/10.5194/bg-16-3247-2019, 2019.

IPCC: Climate Change 2007: The Physical Science Basis. Contribution of Working Group I to the Fourth Assessment Report of the Intergovernmental Panel on Climate Change, IPCC, Geneva, 2007.

Jinuntuya-Nortman, M., Sutka, R. L., Ostrom, P. H., Gandhi, H., and Ostrom, N. E.: Isotopologue fractionation during microbial reduction of N_2O within soil mesocosms as a function of water-filled pore space, Soil Biol. Biochem., 40, 2273–2280, 2008.

Kato, T., Toyoda, S., Yoshida, N., Tang, Y. H., and Wada, E.: Isotopomer and isotopologue signatures of N_2O produced in alpine ecosystems on the Qinghai-Tibetan Plateau, Rapid Commun. Mass Sp., 27, 1517–1526, 2013.

Knowles, R.: Denitrification, Microbiol. Rev., 46, 43–70, 1982.

Koba, K., Osaka, K., Tobari, Y., Toyoda, S., Ohte, N., Katsuyama, M., Suzuki, N., Itoh, M., Yamagishi, H., Kawasaki, M., Kim, S. J., Yoshida, N., and Nakajimag, T.: Biogeochemistry of nitrous oxide in groundwater in a forested ecosystem elucidated by nitrous oxide isotopomer measurements, Geochim. Cosmochim. Ac., 73, 3115–3133, 2009.

Kool, D. M., Wrage, N., Oenema, O., Dolfing, J., and Van Groenigen, J. W.: Oxygen exchange between (de) nitrification intermediates and H_2O and its implications for source determination of NO_3^- and N_2O: a review, Rapid Commun. Mass Sp., 21, 3569–3578, 2007.

Kool, D. M., Wrage, N., Oenema, O., Harris, D., and Van Groenigen, J. W.: The ^{18}O signature of biogenic nitrous oxide is determined by O exchange with water, Rapid Commun. Mass Sp., 23, 104–108, 2009.

Kramps-Alpmann, D., Ruoss, N., Korte K., Ernst, U., and Schäfer, B. C.: Klimaoptimierte Anpassungsstrategien in der Landwirtschaft (optimierter Klimabetrieb) II., unpublished project report, 2017.

Kulkarni, M. V., Burgin, A. J., Groffman, P. M., and Yavitt, J. B.: Direct flux and ^{15}N tracer methods for measuring denitrification in forest soils, Biogeochemistry, 117, 359–373, 2013.

Lewicka-Szczebak, D. and Well, R.: The ^{15}N gas-flux method to determine N_2 flux : a comparison of different tracer addition approaches, Soil, 6, 145–152, 2020.

Lewicka-Szczebak, D., Well, R., Giesemann, A., Rohe, L., and Wolf, U.: An enhanced technique for automated determination of ^{15}N signatures of N_2, $(N_2 + N_2O)$ and N_2O in gas samples, Rapid Commun. Mass Sp., 27, 1548–1558, 2013.

Lewicka-Szczebak, D., Well, R., Koster, J. R., Fuss, R., Senbayram, M., Dittert, K., and Flessa, H.: Experimental determinations of isotopic fractionation factors associated with N_2O production and reduction during denitrification in soils, Geochim. Cosmochim. Ac., 134, 55–73, 2014.

Lewicka-Szczebak, D., Well, R., Bol, R., Gregory, A., Matthews, P., Misselbrook, T., Whalley, R., and Cardenas, L.: Isotope fractionation factors controlling isotopocule signatures of soil-emitted N_2O produced by denitrification processes of various rates, Rapid Commun. Mass Sp., 29, 269–282, 2015.

Lewicka-Szczebak, D., Dyckmans, J., Kaiser, J., Marca, A., Augustin, J., and Well, R.: Oxygen isotope fractionation during N_2O production by soil denitrification, Biogeosciences, 13, 1129–1144, https://doi.org/10.5194/bg-13-1129-2016, 2016.

Lewicka-Szczebak, D., Augustin, J., Giesemann, A., and Well, R.: Quantifying N_2O reduction to N_2 based on N_2O isotopocules validation with independent methods (helium incubation and ^{15}N gas flux method), Biogeosciences, 14, 711–732, https://doi.org/10.5194/bg-14-711-2017, 2017.

Maeda, K., Spor, A., Edel-Hermann, V., Heraud, C., Breuil, M. C., Bizouard, F., Toyoda, S., Yoshida, N., Steinberg, C., and Philippot, L.: N_2O production, a widespread trait in fungi, Sci. Rep.-UK, 5, 9697, 9691–9697, 2015.

Mandernack, K. W., Mills, C. T., Johnson, C. A., Rahn, T., and Kinney, C.: The $\delta^{15}N$ and $\delta^{18}O$ values of N_2O produced during the co-oxidation of ammonia by methanotrophic bacteria, Chem. Geol., 267, 96–107, 2009.

Mathieu, O., Leveque, J., Henault, C., Milloux, M. J., Bizouard, F., and Andreux, F.: Emissions and spatial variability of N_2O, N_2 and nitrous oxide mole fraction at the field scale, revealed with ^{15}N isotopic techniques, Soil Biol. Biochem., 38, 941–951, 2006.

Menyailo, O. V. and Hungate, B. A.: Stable isotope discrimination during soil denitrification: Production and consumption of nitrous oxide, Global Biogeochem. Cy., 20, GB3025, https://doi.org/10.1029/2005GB002527, 2006.

Mohn, J., Wolf, B., Toyoda, S., Lin, C. T., Liang, M. C., Bruggemann, N., Wissel, H., Steiker, A. E., Dyckmans, J., Szwec, L., Ostrom, N. E., Casciotti, K. L., Forbes, M., Giesemann, A., Well, R., Doucett, R. R., Yarnes, C. T., Ridley, A. R., Kaiser, J., and Yoshida, N.: Interlaboratory assessment of nitrous oxide isotopomer analysis by isotope ratio mass spectrometry and laser spectroscopy: current status and perspectives, Rapid Commun. Mass Sp., 28, 1995–2007, 2014.

Moore, J. W. and Semmens, B. X.: Incorporating uncertainty and prior information into stable isotope mixing models, Ecology Letters, 11, 470–480, 2008.

Morse, J. L. and Bernhardt, E. S.: Using ^{15}N tracers to estimate N_2O and N_2 emissions from nitrification and denitrification in coastal plain wetlands under contrasting land-uses, Soil Biol. Biochem., 57, 635–643, 2013.

Mosier, A. R., Guenzi, W. D., and Schweizer, E. E.: Field Denitrification Estimation by N-15 and Acetylene Inhibition Techniques, Soil Sci. Soc. Am. J,. 50, 831–833, 1986.

Müller, C., Laughlin, R. J., Spott, O., and Rütting, T.: Quantification of N_2O emission pathways via a ^{15}N tracing model, Soil Biol. Biochem., 72, 44–54, 2014.

Nash, J. E. and Sutcliffe, J. V.: River flow forecasting through conceptual models part I – a discussion of principles, J. Hydrol., 10, 282–290, 1970.

Opdyke, M. R., Ostrom, N. E., and Ostrom, P. H.: Evidence for the predominance of denitrification as a source of N_2O in temperate agricultural soils based on isotopologue measurements, Global Biogeochem. Cy., 23, GB4018, 4011–4010, 2009.

Ostrom, N. E., Pitt, A., Sutka, R., Ostrom, P. H., Grandy, A. S., Huizinga, K. M., and Robertson, G. P.: Isotopologue effects during N_2O reduction in soils and in pure cultures of denitrifiers, J. Geophys. Res.-Biogeo., 112, G02005, 02001–02012, 2007.

Ostrom, N. E., Sutka, R., Ostrom, P. H., Grandy, A. S., Huizinga, K. M., Gandhi, H., von Fischer, J. C., and Robertson, G. P.: Isotopologue data reveal bacterial denitrification as the primary source of N_2O during a high flux event following cultivation of a native temperate grassland, Soil Biol. Biochem., 42, 499–506, 2010.

Park, S., Perez, T., Boering, K. A., Trumbore, S. E., Gil, J., Marquina, S., and Tyler, S. C.: Can N_2O stable isotopes and isotopomers be useful tools to characterize sources and microbial pathways of N_2O production and consumption in tropical soils?, Global Biogeochem. Cy., 25, GB1001, https://doi.org/10.1029/2009GB003615, 2011.

Parnell, A. C., Phillips, D. L., Bearhop, S., Semmens, B. X., Ward, E. J., Moore, J. W., Jackson, A. L., Grey, J., Kelly, D. J., and Inger, R.: Bayesian stable isotope mixing models, Environmetrics, 24, 387–399, 2013.

Phillips, D. L., Inger, R., Bearhop, S., Jackson, A. L., Moore, J. W., Parnell, A. C., Semmens, B. X., and Ward, E. J.: Best practices for use of stable isotope mixing models in food-web studies, Can. J. Zool., 92, 823–835, 2014.

Ravishankara, A. R., Daniel, J. S., and Portmann, R. W.: Nitrous Oxide (N_2O): The Dominant Ozone-Depleting Substance Emitted in the 21st Century, Science, 326, 123–125, 2009.

Röckmann, T., Kaiser, J., Brenninkmeijer, C. A. M., and Brand, W. A.: Gas chromatography/isotope-ratio mass spectrometry method for high-precision position-dependent ^{15}N and ^{18}O measurements of atmospheric nitrous oxide, Rapid Commun. Mass Sp., 17, 1897–1908, 2003.

Rohe, L., Anderson, T.-H., Braker, G., Flessa, H., Giesemann, A., Lewicka-Szczebak, D., Wrage-Mönnig, N., and Well, R.: Dual isotope and isotopomer signatures of nitrous oxide from fungal denitrification – a pure culture study, Rapid Commun. Mass Sp., 28, 1893–1903, 2014a.

Rohe, L., Anderson, T. H., Braker, G., Flessa, H., Giesemann, A., Wrage-Monnig, N., and Well, R.: Fungal oxygen exchange between denitrification intermediates and water, Rapid Commun. Mass Sp., 28, 377–384, 2014b.

Rohe, L., Well, R., and Lewicka-Szczebak, D.: Use of oxygen isotopes to differentiate between nitrous oxide produced by fungi or bacteria during denitrification, Rapid Commun. Mass Sp., 31, 1297–1312, 2017.

Saggar, S., Jha, N., Deslippe, J., Bolan, S., Luo, J., Giltrap, D. L., Kim, D.-G., Zaman, M., and Tillman, R. W.: Denitrification and N_2O:N_2 production in temperate grasslands: Processes, measurements, modelling and mitigating negative impacts, Sci. Total Environ., 465, 173–195, 2013.

Schmidt, G., Segschneider H.-J., and R., R.: Bestimmung der ^{15}N Häufigkeit bei nichtstatistischer ^{15}N-verteilung in N_2 sowie bei N_2O in Bodenluftproben mittels GC-R-IRMS-Kopplung in einem Probenlauf, Isot. Environ. Healt S., 34, 235–243, 1998.

Scholefield, D., Hawkins, J. M. B., and Jackson, S. M.: Development of a helium atmosphere soil incubation technique for direct measurement of nitrous oxide and dinitrogen fluxes during denitrification, Soil Biol. Biochem., 29, 1345–1352, 1997.

Seitzinger, S.: Nitrogen cycle – Out of reach, Nature, 452, 162–163, 2008.

Senbayram, M., Chen, R., Budai, A., Bakken, L., and Dittert, K.: N_2O emission and the $N_2O/(N_2O+N_2)$ product ratio of denitrification as controlled by available carbon substrates and nitrate concentrations, Agr. Ecosyst. Environ., 147, 4–12, 2012.

Sigman, D. M., Casciotti, K. L., Andreani, M., Barford, C., Galanter, M., and Bohlke, J. K.: A bacterial method for the nitrogen isotopic analysis of nitrate in seawater and freshwater, Anal. Chem., 73, 4145–4153, 2001.

Spott, O., Russow, R., Apelt, B., and Stange, C. F.: A N-15-aided artificial atmosphere gas flow technique for online determination of soil N_2 release using the zeolite Kostrolith SX6 (R), Rapid Commun. Mass Sp., 20, 3267–3274, 2006.

Stange, C. F., Spott, O., Apelt, B., and Russow, R. W. B.: Automated and rapid online determination of ^{15}N abundance and concentration of ammonium, nitrite, or nitrate in aqueous samples by the SPINMAS technique, Isot. Environ. Healt S., 43, 227–236, 2007.

Stevens, R. J. and Laughlin, R. J.: Nitrite Transformations during Soil Extraction with Potassium-Chloride, Soil Sci. Soc. Am. J., 59, 933–938, 1995.

Sutka, R. L., Ostrom, N. E., Ostrom, P. H., Breznak, J. A., Gandhi, H., Pitt, A. J., and Li, F.: Distinguishing nitrous oxide production from nitrification and denitrification on the basis of isotopomer abundances, Appl. Environ. Microb., 72, 638–644, 2006.

Sutka, R. L., Adams, G. C., Ostrom, N. E., and Ostrom, P. H.: Isotopologue fractionation during N_2O production by fungal denitrification, Rapid Commun. Mass Sp., 22, 3989–3996, 2008.

Toyoda, S. and Yoshida, N.: Determination of nitrogen isotopomers of nitrous oxide on a modified isotope ratio mass spectrometer, Anal. Chem., 71, 4711–4718, 1999.

Toyoda, S., Mutobe, H., Yamagishi, H., Yoshida, N., and Tanji, Y.: Fractionation of N_2O isotopomers during production by denitrifier, Soil Biol. Biochem., 37, 1535–1545, 2005.

Toyoda, S., Yano, M., Nishimura, S., Akiyama, H., Hayakawa, A., Koba, K., Sudo, S., Yagi, K., Makabe, A., Tobari, Y., Ogawa, N. O., Ohkouchi, N., Yamada, K., and Yoshida, N.: Characterization and production and consumption processes of N_2O emitted from temperate agricultural soils determined via isotopomer ratio analysis, Global Biogeochem. Cy., 25, GB2008, https://doi.org/10.1029/2009GB003769, 2011.

Toyoda, S., Yoshida, N., and Koba, K.: Isotopocule analysis of biologically produced nitrous oxide in various environments, Mass Spectrom. Rev., 36, 135–160, https://doi.org/10.1002/mas.21459, 2017.

Verhoeven, E., Barthel, M., Yu, L., Celi, L., Said-Pullicino, D., Sleutel, S., Lewicka-Szczebak, D., Six, J., and Decock, C.: Early season N_2O emissions under variable water management in rice systems: source-partitioning emissions using isotope ratios along a depth profile, Biogeosciences, 16, 383–408, https://doi.org/10.5194/bg-16-383-2019, 2019.

Wei, J., Ibraim, E., Brüggemann, N., Vereecken, H., and Mohn, J.: First real-time isotopic characterisation of N_2O from chemodenitrification, Geochim. Cosmochim. Ac., 267, 17–32, 2019.

Well, R. and Flessa, H.: Isotope fractionation factors of N_2O diffusion, Rapid Commun. Mass Sp., 22, 2621–2628, 2008.

Well, R. and Flessa, H.: Isotopologue enrichment factors of N_2O reduction in soils, Rapid Commun. Mass Sp., 23, 2996–3002, 2009.

Well, R., Eschenbach, W., Flessa, H., von der Heide, C., and Weymann, D.: Are dual isotope and isotopomer ratios of N_2O useful indicators for N_2O turnover during denitrification in nitrate-contaminated aquifers?, Geochim. Cosmochim. Ac., 90, 265–282, 2012.

Well, R., Burkart, S., Giesemann, A., Grosz, B., Köster, J. R., and Lewicka-Szczebak, D.: Improvement of the ^{15}N gas flux method for in situ measurement of soil denitrification and its product stoichiometry, Rapid Commun. Mass Sp., 33, 437–448, 2019a.

Well, R., Maier, M., Lewicka-Szczebak, D., Köster, J.-R., and Ruoss, N.: Underestimation of denitrification rates from field application of the ^{15}N gas flux method and its correction by gas diffusion modelling, Biogeosciences, 16, 2233–2246, https://doi.org/10.5194/bg-16-2233-2019, 2019b.

Westley, M. B., Popp, B. N., and Rust, T. M.: The calibration of the intramolecular nitrogen isotope distribution in nitrous oxide measured by isotope ratio mass spectrometry, Rapid Commun. Mass Sp., 21, 391–405, 2007.

Wolf, B., Merbold, L., Decock, C., Tuzson, B., Harris, E., Six, J., Emmenegger, L., and Mohn, J.: First on-line isotopic characterization of N_2O above intensively managed grassland, Biogeosciences, 12, 2517–2531, https://doi.org/10.5194/bg-12-2517-2015, 2015.

Wrage-Mönnig, N., Horn, M. A., Well, R., Müller, C., Velthof, G., and Oenema, O.: The role of nitrifier denitrification in the production of nitrous oxide revisited, Soil Biol. Biochem., 123, A3–A16, 2018.

Wu, D., Well, R., Cárdenas, L. M., Fuß, R., Lewicka-Szczebak, D., Köster, J. R., Brüggemann, N., and Bol, R.: Quantifying N_2O reduction to N_2 during denitrification in soils via isotopic mapping approach: Model evaluation and uncertainty analysis, Environ. Res., 2019, 108806, https://doi.org/10.1016/j.envres.2019.108806, 2019.

Wu, H. H., Dannenmann, M., Fanselow, N., Wolf, B., Yao, Z. S., Wu, X., Bruggemann, N., Zheng, X. H., Han, X. G., Dittert, K., and Butterbach-Bahl, K.: Feedback of grazing on gross rates of N mineralization and inorganic N partitioning in steppe soils of Inner Mongolia, Plant Soil, 340, 127–139, 2011.

Yamagishi, H., Westley, M. B., Popp, B. N., Toyoda, S., Yoshida, N., Watanabe, S., Koba, K., and Yamanaka, Y.: Role of nitrification and denitrification on the nitrous oxide cycle in the eastern tropical North Pacific and Gulf of California, J. Geophys. Res.-Biogeo., 112, https://doi.org/10.1029/2006JG000227, 2007.

Yoshida, N.: ^{15}N-depleted N_2O as a product of nitrification, Nature, 335, 528–529, 1988.

Yu, L., Harris, E., Lewicka-Szczebak, D., Barthel, M., Blomberg, M. R. A., Harris, S., Johnson, M. S., Lehmann, M. F., Liisberg, J., Müller, C., Ostrom, N., Six, J., Toyoda, S., Yoshida, N., and Mohn, J.: What can we learn from N_2O isotope data? – Analytics, processes and modelling, Rapid Commun. Mass Sp., 34, e8858, https://doi.org/10.1002/rcm.8858, 2020.

Zhang, J. B., Muller, C., and Cai, Z. C.: Heterotrophic nitrification of organic N and its contribution to nitrous oxide emissions in soils, Soil Biol. Biochem., 84, 199–209, 2015.

Zhang, L., Altabet, M. A., Wu, T. X., and Hadas, O.: Sensitive measurement of NH_4^+ $^{15}N/^{14}N$ ($\delta^{15}NH_4^+$) at natural abundance levels in fresh and saltwaters, Anal. Chem., 79, 5297–5303, 2007.

Zou, Y., Hirono, Y., Yanai, Y., Hattori, S., Toyoda, S., and Yoshida, N.: Isotopomer analysis of nitrous oxide accumulated in soil cultivated with tea (Camellia sinensis) in Shizuoka, central Japan, Soil Biol. Biochem., 77, 276–291, 2014.